Therapeutic remodeling of CBP transcription factor complex controls oncogenic gene expression in acute myeloid leukemia

Lauren Forbes[1,4], Paolo Cifani[1], Gerard Minuesa[1], Celine Chen[1], Sumiko Takao[1], Michael G Kharas[1,4], Richard P. Koche[3], Alex Kentsis [1,2,4,5*]

[1] Molecular Pharmacology Program, Sloan Kettering Institute, New York, NY 10065, USA.
[2] Department of Pediatrics, Memorial Sloan Kettering Cancer Center, New York 10065, NY, USA.
[3] Center for Epigenetics Research, Sloan Kettering Institute, New York, NY 10065, USA.
[4] Departments of Pharmacology and Physiology & Biophysics, Weill Cornell Medical College, Cornell University, New York, NY 10065, USA.
[5] Lead Contact

* Correspondence: kentsisresearchgroup@gmail.com, @KentsisResearch

HIGHLIGHTS

- Cell-penetrant peptidomimetic inhibitor selectively blocks oncogenic MYB:CBP/P300 activity in diverse leukemias but not normal blood cells
- MYB assembles aberrant transcription factor complexes in AML required for programming leukemic gene expression
- CBP/P300 sequestration contributes to MYB-dependent leukemogenic gene expression and chromatin organization

SUMMARY

Dysregulated gene expression is one of the most prevalent features in human cancers. Here, we show that most subtypes of acute myeloid leukemia (AML) depend on the aberrant assembly of the MYB transcriptional co-activator complex. By rapid and selective peptidomimetic interference with the binding of CBP/P300 to MYB, but not CREB or MLL, we find that the leukemic functions of MYB are mediated by CBP/P300-mediated co-activation of a distinct set of transcriptional factor complexes that are aberrantly assembled with MYB in AML cells. This therapeutic remodeling is accompanied by dynamic redistribution of CBP/P300 complexes to genes that control cellular differentiation and growth. We propose that convergently organized transcription factor complexes in AML cells control oncogenic gene expression programs. These findings establish a compelling strategy for pharmacologic reprogramming of oncogenic gene expression that supports its targeting for leukemias and possibly other human cancers caused by dysregulated gene control.

INTRODUCTION

Gene dysregulation is one of the most prevalent features in human cancers (Bradner, Hnisz and Young, 2017). In many tumors, this is due to the pathogenic mutations of promoters, enhancers, and genes encoding either transcription factors or factors that regulate chromatin and gene expression. In blood cancers, and acute myeloid leukemias (AML) in particular, aberrant gene expression is thought to contribute to most key properties of leukemia cells, including self-renewal, growth, and resistance to therapy. For example, numerous pathogenic chromosomal translocations in AML, such as those involving *AML1* (*RUNX1*) and *MLL* (*KMT2A*) produce chimeric transcription or chromatin remodeling factors that cause disease (Look, 1997). Consequently, therapeutic strategies aimed at restoring normal gene expression are compelling because of their ability to target the causal molecular processes and induce leukemia cell differentiation and elimination, leading to durable disease control.

While specific molecular dependencies have been identified for some genetic subtypes of AML, such as DOT1L or Menin inhibition for *MLL*-rearranged leukemias (Krivtsov *et al.*, 2019), and CARM1 inhibition for *AML1*-rearranged leukemias (Greenblatt *et al.*, 2019), distinct pathogenetic mechanisms of diverse AML subtypes also appear to converge on shared molecular pathways. For example, approximately 25% of adult and childhood AMLs, including both *MLL*-rearranged and non-rearranged cases, require aberrant activation of the transcription factor MEF2C, conferring susceptibility to MARK and SIK inhibitors, which are currently being explored for clinical trials for patients (Brown *et al.*, 2018; Tarumoto *et al.*, 2018; Vakoc and Kentsis, 2018). Similarly, nearly 50% of examined AML specimens exhibit aberrant activation of HGF/MET/FGFR signaling (Kentsis *et al.*, 2012), as being currently tested in the ongoing clinical trial of combined MET and FGFR inhibitors in patients with relapsed or refractory AML (ClinicalTrials.gov Identifier NCT03125239). Even for therapies targeting leukemogenic proteins directly, such as inhibitors of IDH1/2, FLT3, KIT, SYK, as well as epigenetic and apoptotic therapies such as decitabine and venetoclax, their therapeutic efficacy and resistance depend on the underlying gene expression phenotypic states of AML cells (Tyner *et al.*, 2018). Thus, there is intense interest in defining shared molecular dependencies controlling leukemogenic gene expression in AML that can provide effective therapeutic options for patients.

Recently, MYB has been nominated as a therapeutic target in AML, as transient suppression of *Myb* nearly completely eliminates leukemia development in mouse models *in vivo* while sparing normal hematopoietic cells (Zuber, Rappaport, et al., 2011). Indeed, pioneering studies have implicated Myb as a key mediator of leukemias (Klempnauer and Bishop, 1984; Luger *et al.*, 2002). MYB is the cellular homologue of the viral *v-Myb* oncogene that can cause avian leukemias and function as a pioneer transcription factor in mammalian cells (Biedenkapp et al., 1988). MYB functions as a master regulator of gene expression in various cell types, including hematopoietic cells where it controls cell proliferation and differentiation (Ramsay and Gonda, 2008). Both mutations and translocations of *MYB* have causal roles in various human malignancies, including leukemias. For example, aberrant expression of *TAL1* in T-cell acute lymphoid leukemia (T-ALL) is induced by pathogenic somatic mutations that create neomorphic MYB binding sites (Mansour et al., 2014). Likewise, *MYB* is recurrently rearranged in distinct subtype of blastic plasmacytoid dendritic cell neoplasms (BPDCN), a highly refractory hematologic malignancy (Suzuki *et al.*, 2017).

Notably, the *Booreana* strain of mice that impairs the binding of Myb by its co-activator CBP/P300 (Crebbp/Ep300) due to the mutation of Myb E308G in its transcriptional activation domain, is resistant to leukemogenesis induced by the otherwise fully penetrant *MLL-AF9* and *AML1-ETO* oncogenes, but has largely normal hematopoiesis (Pattabiraman *et al.*, 2014). Altogether, these findings indicate that MYB and its co-factor CBP/P300 are fundamentally dysregulated in AML, presumably through disordered gene expression that characterizes most

forms of AML. However, the specific details of this mechanism remain poorly understood, largely due to the lack of suitable tools.

Recently, we developed a peptidomimetic inhibitor of MYB:CBP/P300 (Ramaswamy *et al.*, 2018). Here, we report its second-generation version that has significantly increased potency, and consequently suppresses leukemic MYB functions in most AML subtypes tested, while sparing normal hematopoietic progenitor cells. By rapid and selective peptidomimetic interference with the binding of CBP/P300 to MYB, but not CREB or MLL, we find that the leukemic functions of MYB are mediated by CBP/P300-mediated co-activation of a distinct set of transcriptional factor complexes that are aberrantly assembled with MYB in AML cells. This therapeutic remodeling is accompanied by dynamic redistribution of CBP/P300 complexes to genes that control cellular differentiation and growth. These findings establish a compelling strategy for pharmacologic reprogramming of oncogenic gene expression that should lead to improved therapies for leukemias and other human cancers caused by dysregulated gene control.

RESULTS

CRYBMIM is a peptidomimetic chimera that specifically binds CBP/P300 KIX domain

Of all the functional genetic dependencies examined to date, the transcription factor *MYB* demonstrates the broadest dependency across diverse AML subtypes, as compared to other non-hematopoietic cancers (Tarumoto *et al.*, 2018). To generalize this analysis, we queried 652 human cancer cell lines tested as part of the DepMap Cancer Dependency Map to identify genes that are selectively required for the growth and survival of leukemia as compared to other cancer types. We found that *MYB* is the most significantly required human gene in 37 leukemia cell lines, including 20 AML cell lines, of diverse molecular subtypes (p = 1.1e-15; Figure 1A).

MYB target gene activation requires its specific interaction with CREB-binding protein (CBP)/P300 for co-activation (Dai *et al.*, 1996). The helical MYB transactivation domain comprising residues 293-310 binds to the KIX domain of CBP/P300 (Zor *et al.*, 2004). Using molecular mechanics simulations, we previously developed a peptidomimetic inhibitor of this interaction, termed MYBMIM (Ramaswamy *et al.*, 2018). MYBMIM uses stereoselective substitution of D-amino acids to confer proteolytic stability, and the cationic TAT domain for cell penetration. As a result, MYBMIM can specifically inhibit MYB:CBP/P300 binding in cells, but its activity less pronounced in non-MLL-rearranged AML cells. Given that MYBMIM bound to recombinant CBP KIX domain with the dissociation constant of 21.3 ± 2.9 μM, as compared to the native MYB peptide of 4.2 ± 0.5 μM (Ramaswamy *et al.*, 2018), we reasoned that a peptidomimetic inhibitor with higher affinity to CBP/P300 would be more effective.

Consequently, we used molecular modeling to extend MYBMIM into the adjoining binding site that binds CREB (Radhakrishnan et al., 1997; Cheng et al., 2008). We appended CREB residues 124-147 to MYBMIM, while replacing the EKIRK motif to maintain favorable backbone geometry, as confirmed by molecular energy minimization calculations in implicit solvent (Figures 1B, 1C and S1). Termed CRYBMIM, this design preserves key MYB residues implicated in leukemic transformation, including E308 which forms a salt bridge with CBP H602, while including the pS133-containing portion of CREB that is responsible for its high affinity binding to CBP (Zor *et al.*, 2004)(Radhakrishnan *et al.*, 1997; Cheng *et al.*, 2008). Similarly, we also designed two additional peptidomimetic inhibitors targeting the distinct CREB and MLL1 binding sites that are proximal to but non-overlapping with the MYB binding site, termed CREBMIM and MLLMIM, respectively (Figures 1B, 1C and S1).

As expected, both CRYBMIM and CREBMIM bind to the purified recombinant CBP KIX domain with significantly improved (3-6 fold) affinities as compared to MYBMIM and measured by microscale thermophoresis (K_d of 5.7 ± 0.2 μM, 2.9 ± 0.7 μM, and 17.3 ± 1.6 μM, p = 1e-15; Figure 1D). To confirm these peptides can bind the CBP/P300 complex from cells, we immobilized biotinylated CRYBMIM and CREBMIM peptides on streptavidin beads and used them to affinity purify CBP/P300 from native nuclear extracts of MV411 AML cells. Consistently, we observed efficient binding of nuclear CBP/P300 to peptide-conjugated but not control streptavidin beads (Figure 1E). We found that increasing concentrations of free CRYBMIM could compete with the binding of CBP/P300 to immobilized CRYBMIM, with the apparent K_i of approximately 4.7 μM based on quantitative fluorescence densitometry measurements (Figure 1F). We confirmed the specificity of this binding by incubating bound complexes with 100-fold excess of TAT control peptides, which demonstrated no measurable displacement as compared to PBS control (Figure 1E-F). In contrast, excess CREBMIM was significantly less effective at displacing CBP/P300 from immobilized CREBMIM (apparent K_i > 100 μM, Figure 1E-F), consistent with the much higher nM affinity and allosteric effects that characterize the CREB:CBP/P300 interaction (Radhakrishnan *et al.*, 1997; Goto *et al.*, 2002). Thus, CRYBMIM is a specific high-affinity inhibitor of MYB:CBP/P300 binding.

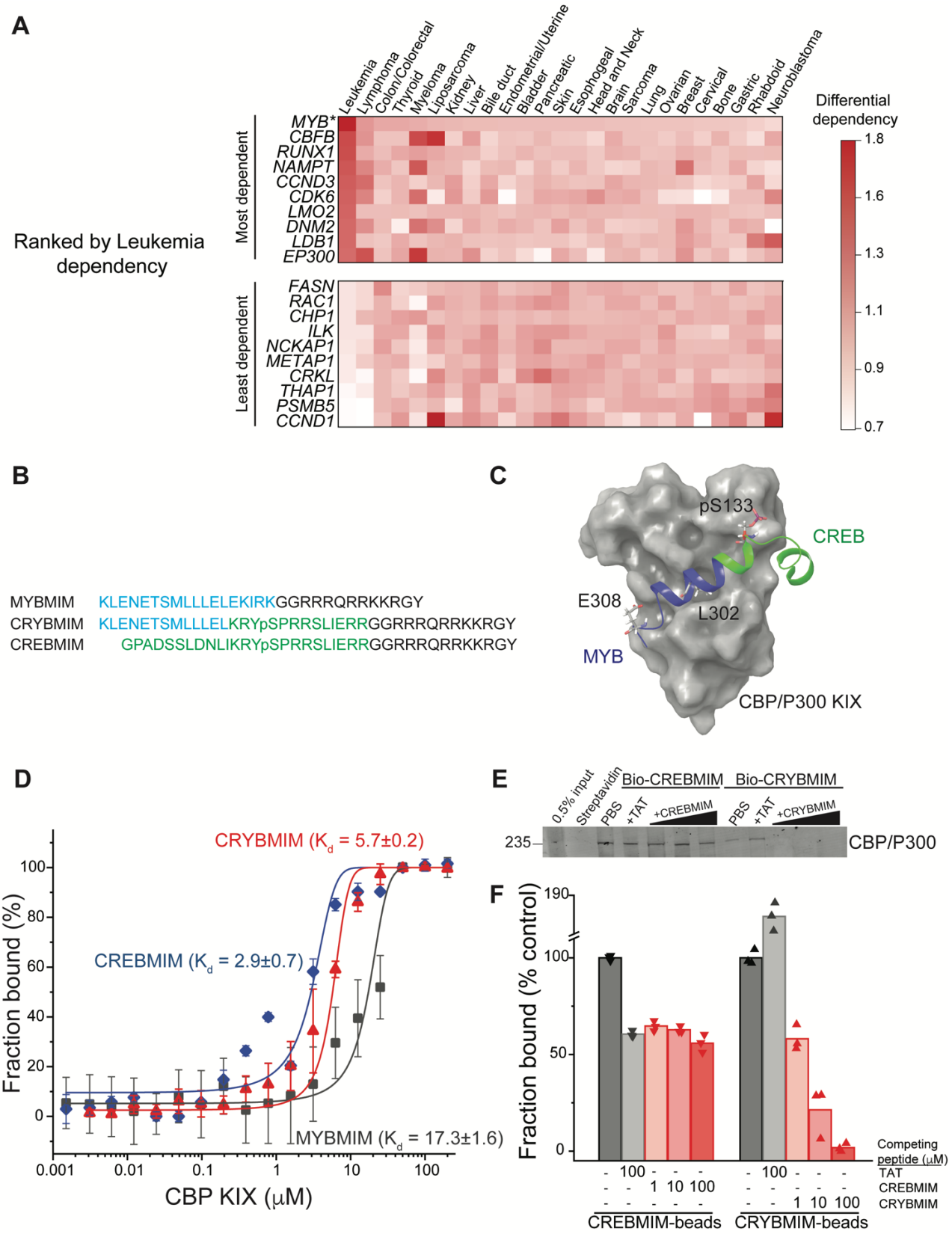

Potent and broad-spectrum activity of CRYBMIM against diverse subtypes of AML

To confirm that CRYBMIM maintains effective cell penetration and nuclear accumulation in AML cells, we studied its fluorescein isothiocyanate (FITC)-conjugated derivative using live cell confocal fluorescence microscopy (Figure 2A). Consistently, we observed that both FITC-CRYBMIM and FITC-CREBMIM efficiently localized to the nuclei of MV411 AML cells within one hour of peptide treatment (Figure 2A). We confirmed specific nuclear accumulation of CRYBMIM as opposed to non-specific membrane binding that can affect TAT-containing peptides by confocal sub-cellular imaging of cells co-stained with specific mitochondrial and nuclear dyes (Figure 2A).

Previously, we observed that MYBMIM blocks the binding of MYB to the CBP/P300 in AML cells, requiring relatively high 20 μM concentrations for 3 hours to achieve this effect (Ramaswamy *et al.*, 2018). To ascertain whether CRYBMIM can achieve more potent interference with the binding of MYB to the CBP/P300 complex in cells due to its improved affinity as compared to MYBMIM (Figure 1D), we treated MV411 cells with 10 μM peptides for one hour and immunoprecipitated CBP/P300 using specific antibodies (Figure 2B). Under these more stringent conditions, we found that CRYBMIM is indeed more potent compared to MYBMIM, as evidenced by the substantial depletion of MYB from the immunoprecipitated CBP/P300 complex (Figure 2B).

This effect was specific because the inactive analogue of CRYBMIM, termed CG3, in which 3 key residues have been replaced with glycines, (Table S1), was unable to compete with MYB:CBP/P300 binding in cells, an effect observed with CBP/P300-specific but not control isotype non-specific antibodies (Figure 2B). Neither CREBMIM nor CRYBMIM treatment interfered with the binding of CREB to the cellular CBP/P300 complex (Figure 2B), in agreement with the affinities of their direct binding to the recombinant CBP KIX domain (Figures 1D-F), the nM affinity of CREB:CBP/P300 interaction (Radhakrishnan *et al.*, 1997), and the specific molecular features required for MYB but not CREB or MLL1 binding (Figure 1C and S1).

To test the prediction that higher affinity binding of CRYBMIM to CBP/P300 would translate into improved anti-leukemia potency, we assessed its effects on the viability of cultured human leukemia and normal hematopoietic cells. Consistent with this prediction, we observed that CRYBMIM exhibited significantly higher potency against MV411 AML cells, as compared to CREBMIM and MLLMIM (IC_{50} = 6.9 ± 3.4 μM, 29.2 ± 3.8 μM, and 24.2 ± 2.0 μM, p = 1e-15; Figure 2C). We confirmed CRYBMIM's specificity by analyzing its inactive analogue CG3 and MYBMIM's inactive analogue TG3, in which 3 residues forming key electrostatic and hydrophobic interactions with the KIX domain were replaced by glycines; both exhibited significantly reduced activity (IC_{50} of 16.7 ± 1.0 μM and 48.9 ± 2.6 μM, p = 2.75e-4 and <1e-15, respectively; Figure 2D). Likewise, CRYBMIM exhibited significantly higher activity against MV411 AML cells as compared to the normal human CD34+ umbilical cord progenitor cells (IC_{50} of 12.8 ± 3.6 μM, p = 1.1e-8; Figure 2E).

Importantly, CRYBMIM achieved significantly improved, logarithmic suppression of growth and survival of most AML cell lines tested, as compared to MYBMIM and CREBMIM (Figure 2F). For example, whereas MYBMIM induced nearly 100-fold suppression of growth of MV411 cells after six days of treatment in agreement with prior studies (Ramaswamy *et al.*, 2018), CRYBMIM achieved more than 1,000-fold suppression compared to control (p = 8.6e-3; Figure 2F), consistent with its improved biochemical affinity (Figure 1D). This improved activity of CRYBMIM spanned diverse *MLL*-rearranged and non-*MLL*-rearranged AML subtypes, *AML1-ETO* translocated, *PML-RARA*-translocated, *DNMT3A*-mutant, *NPM1c*-mutant, *TP53*-mutant, *MYC*-amplified, and *WT1*-mutant cell lines, with the exception of erythroblastic *BCR-ABL1*-translocated K562 cells (10 of 11 cell lines tested; Figure 2F and Table S2). In contrast, under these conditions, CRYBMIM had no significant effects on the growth and differentiation of normal human umbilical cord progenitor cells *in vitro* (Figure S2). Thus, CRYBMIM has broad spectrum activity against diverse subtypes of AML but not normal hematopoietic cells.

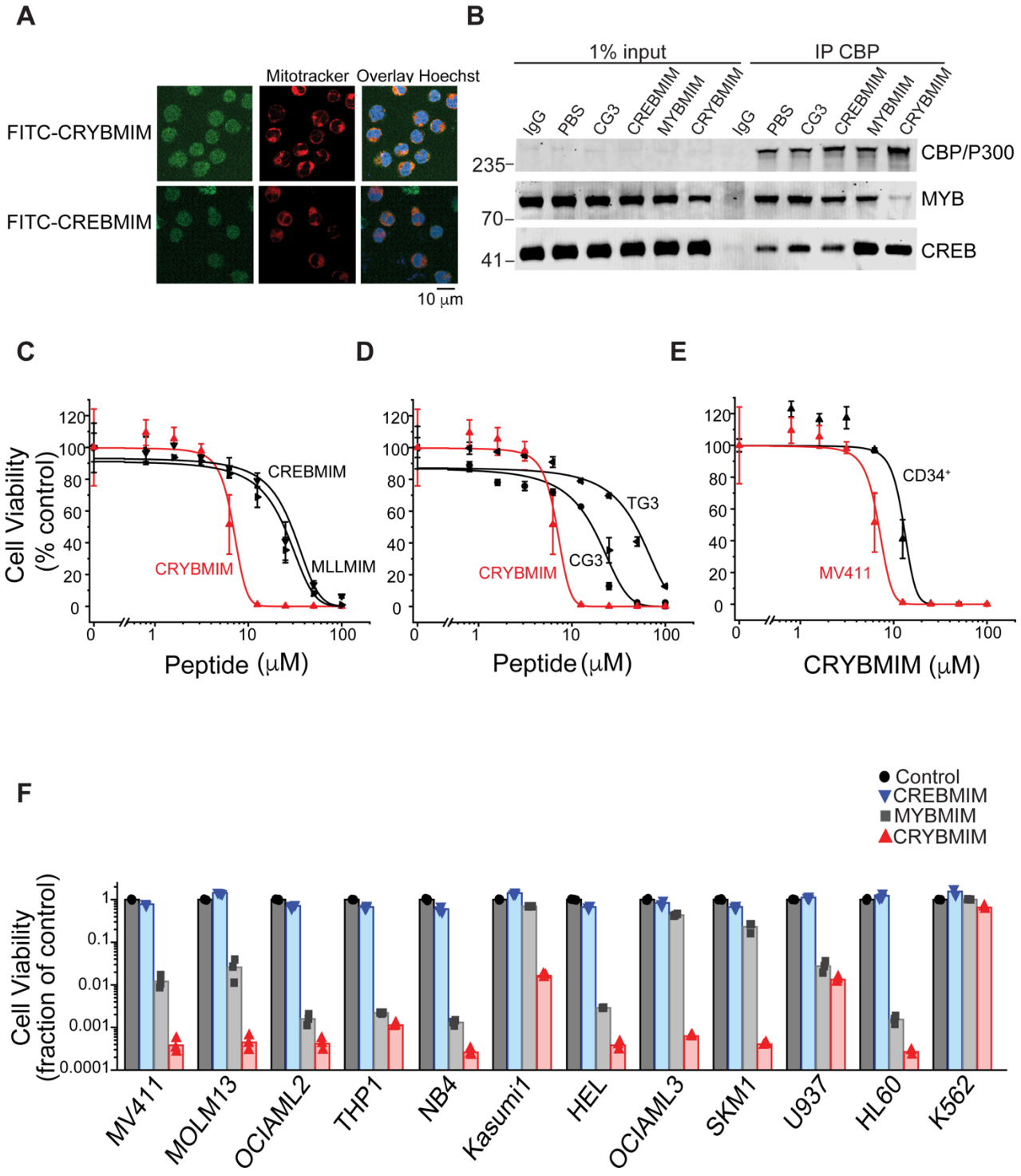

CRYBMIM blocks oncogenic MYB gene expression and restores normal myeloid cell differentiation

The assembly of MYB with CBP/P300 controls gene expression in part due to its transcriptional co-activation at specific enhancers and promoters (Kasper *et al.*, 2010; Zhao *et al.*, 2011). Previously, we found that MYBMIM can suppress MYB:CBP/P300-dependent gene expression, leading to AML cell apoptosis that required MYB-mediated suppression of *BCL2* (Ramaswamy *et al.*, 2018). However, because MYBMIM's suppression of gene expression was accompanied by apoptosis and other cellular responses, we were unable to discern the molecular mechanisms that directly dysregulate the activity of the CBP/P300 transcription factor complex in AML cells.

Given that CRYBMIM has increased affinity for CBP/P300 similar to that of native MYB (5.7 ± 0.2 μM and 4.2 ± 0.5 μM, respectively), we reasoned that its improved activity would now permit detailed kinetic studies to define the specific gene expression programs that are aberrantly activated in AML cells. Consistent with this prediction, comparison of the effects of CRYBMIM on gene expression and consequent apoptosis of MV411 cells revealed that one and four hour exposures led to significant changes in gene expression with minimal induction of apoptosis (Figure S3). Thus, we used RNA-sequencing (RNA-seq) to define the changes on gene expression genome-wide upon one and four hour exposures to CRYBMIM as compared to PBS control (Figures 3A-B). We found that after four-hour duration of treatment, CRYBMIM causes significant downregulation of 2,869 genes, including known MYB target genes *MYC, IKZF1, GATA2,* and *KIT* (Figures 3A-3C). Similar to MYBMIM, CRYBMIM also caused significant upregulation of distinct genes, an effect that was substantially more pronounced upon four hours of treatment (4,099 genes; 3A-B). Interestingly, in addition to the expected suppression of MYB target genes (Figure 3C), gene set enrichment analysis also revealed significant induction of myeloid and monocyte differentiation programs (Figures 3D-3E and Table S3). These effects were specific because in contrast to CRYBMIM, CREBMIM treatment exhibited minimal changes in gene expression (Figure S3C), consistent with its inability to disrupt the cellular CBP/P300 complex (Figure 2B). For example, CRYBMIM induced significant increases in the AP-1 family transcription factors *FOS* and *JUN*, as well as *IL6* and *CSF1* that control myeloid differentiation (Figure 3B) (Selvakumaran, Liebermann and Hoffman-Liebermann, 1992; Gonda *et al.*, 1993). In agreement with these findings, CRYBMIM treatment induced significant phenotypic differentiation of MV411 cells, as evidenced by the induction of monocytic CD11b expression, as measured by flow cytometry (Figure 3F-G). While MYBMIM primarily induces apoptosis of MV411 cells, CRYBMIM effects include both apoptosis and differentiation, as evident from flow cytometry analyses (Figure 3G). This suggests that differentiation blockade is directly linked to oncogenic MYB-dependent gene expression in AML.

CBP/P300 sequestration contributes to MYB-dependent leukemogenic gene expression

The direct link between leukemogenic gene expression and differentiation blockade suggests that CRYBMIM not only blocks the assembly of the MYB:CBP/P300 complex, but also induces its remodeling to promote AML differentiation. To test this hypothesis, we analyzed the occupancy of MYB and CBP/P300 genome-wide using chromatin immunoprecipitation followed by sequencing (ChIP-seq). Consistently, we found that CRYBMIM treatment leads to significant redistribution of both MYB and CBP/P300 on chromatin (Figures 4A-D). For example, after one hour of CRYBMIM treatment, both MYB and CBP/P300 are evicted from loci enriched in the MYB-associated DNA-binding motifs (Figures 4A and 4C, lost peaks). By four hours of CRYBMIM treatment, MYB was significantly depleted from 2,587 promoters and enhancers, primarily at sites associated with the MYB DNA-binding motifs, as well as motifs corresponding to NFY, ETS family, AP-1 family, SP1, and CEBPA transcription factors (Figures 4B and 4D). Noticeably, CBP/P300

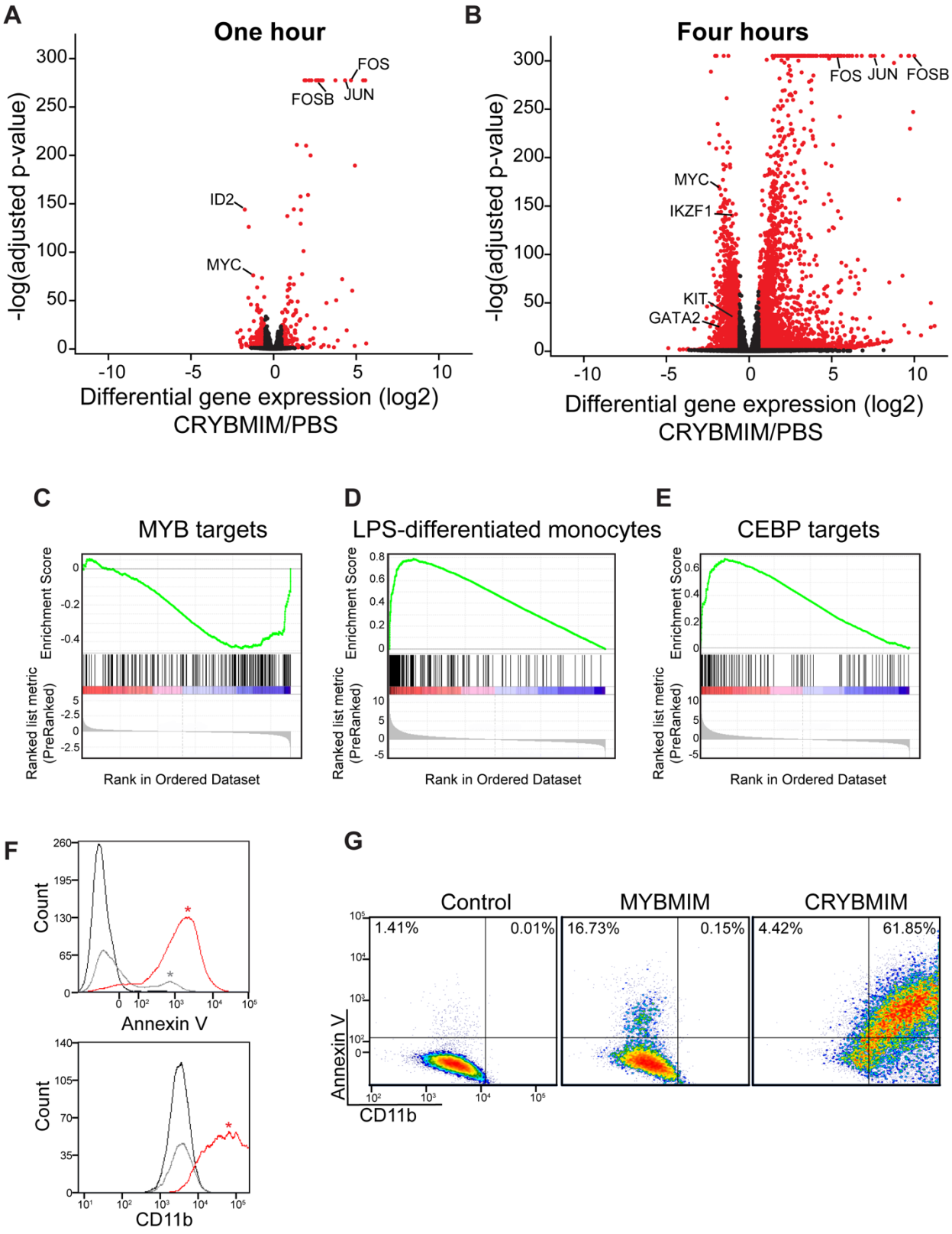

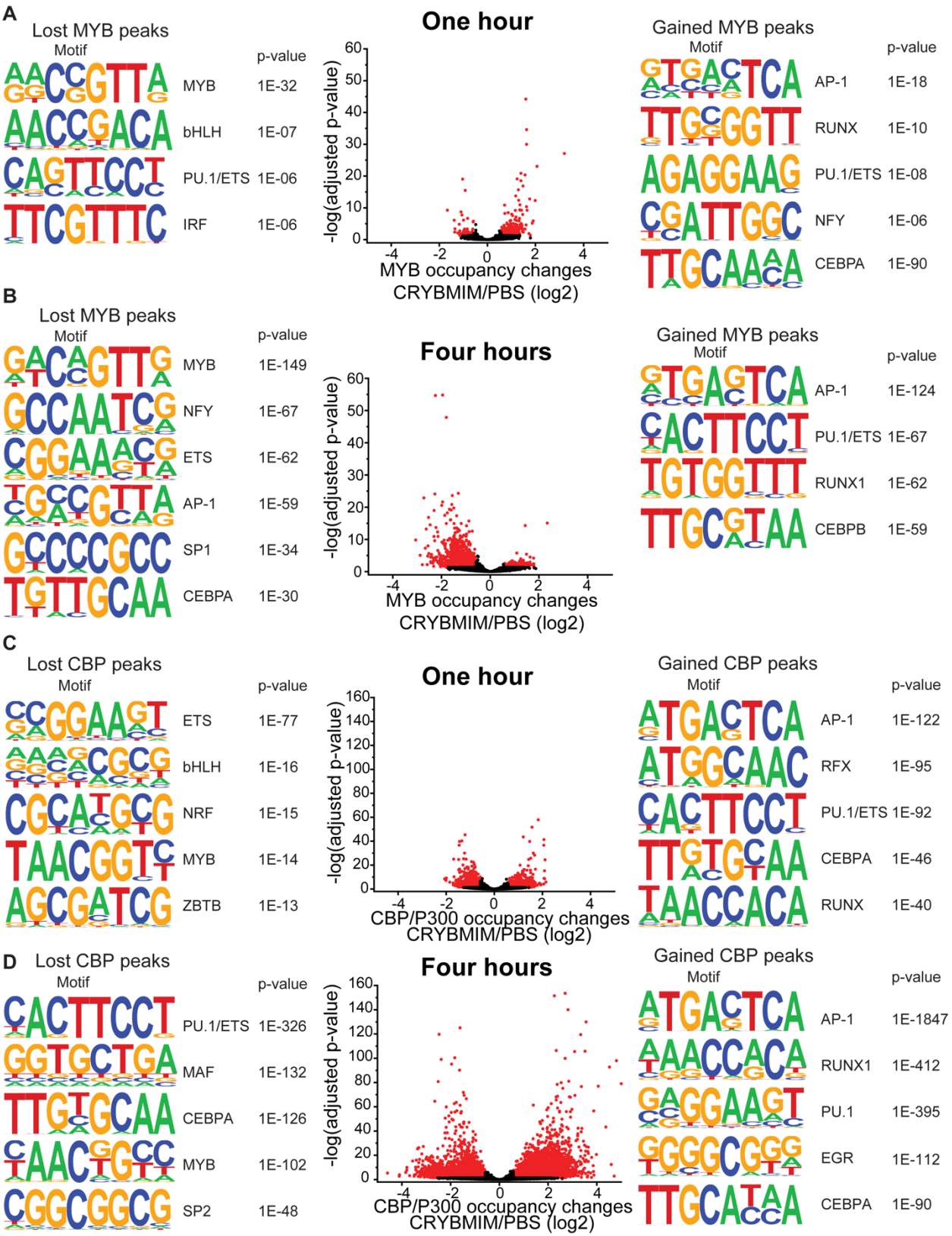

was not only depleted from 7,579 genes, but also significantly redistributed to 11,324 new loci (Figure 4D), consistent with the remodeling of its complex upon CRYBMIM treatment. Loci depleted of CBP/P300 were significantly enriched in MYB-associated DNA-binding motifs, as well as those corresponding to the PU.1, MAF, CEBPA, and SP2 transcription factors (Figure 4D). Likewise, loci that gained CBP/P300 upon CRYBMIM treatment were enriched in DNA-binding motifs for the AP-1, RUNX1, EGR, and CEBPA transcription factors (Figure 4D). In all, peptidomimetic blockade of MYB:CBP/P300 assembly causes remodeling of transcription factor complexes at loci controlling leukemic gene expression, associated with genome-wide redistribution of CBP/P300 transcriptional co-activation complexes. Thus, sequestration of CBP/P300 from genes controlling hematopoietic differentiation contributes to the leukemogenic MYB-dependent gene expression.

MYB assembles aberrant transcription factor complexes in AML cells

Dynamic redistribution of CBP/P300 transcription factor complexes associated with distinct transcription factor activities upon blockade of MYB:CBP/P300 binding suggests that MYB organizes an aberrant transcriptional co-activator complex in AML cells. To define this complex, we used specific antibodies to immunoprecipitate MYB from non-denatured nuclear extracts of MV411 AML cells, and identify co-purifying proteins using high-accuracy quantitative mass spectrometry. To control for abundant proteins and other contaminants that may co-purify non-specifically, we used non-specific isotype control antibodies and precursor ion quantitation to establish stringent statistical parameters that led to the identification of 724 unique proteins that are specifically associated with MYB in MV411 AML cells (Figure 5A). This included CBP itself, as confirmed by the high-confidence identification of unique peptide spectra that distinguish CBP from P300, with four additional peptides shared by both CBP and P300. (Figure S4), as well as other known MYB interactors such as CEBPB (Table S4).

Because MYB is required for the growth and survival of diverse AML subtypes (Figure 1), we reasoned that its essential non-redundant co-factors can be identified from the analysis of their functional dependencies, as assessed by genetic CRISPR interference (Tsherniak *et al.*, 2017). We assigned the CRISPR dependency score of CBP itself in MV411 cells as the threshold to identify functionally non-redundant MYB:CBP co-factors (Figure 5B). We found that these genes encode factors with diverse molecular functions, including a group of 59 chromatin-associated proteins (Table S5). By using currently annotated protein-protein interactions (Oughtred *et al.*, 2019), we constructed their interaction network, based on interactions detected by affinity purifications coupled with either Western immunoblotting or mass spectrometry (Figure 5C). Analysis of their expression in normal human hematopoietic progenitor as compared to AML cells (Cancer Genome Atlas Research Network *et al.*, 2013), led to the identification of candidate co-factors with apparently aberrant expression in AML cells (Figure 5C, dark red). Indeed, 10 such factors were selectively required for 37 leukemia but not 615 other non-hematopoietic cancer cells lines (Figure 5D). The physical association of MYB, CBFB, ZEB2, CEBPA, LYL1, SPI1, RUNX1, LMO2, and GFI1 and their non-redundant functional dependencies in AML cells (Figures 5A-D) are in agreement with the chromatin dynamics involving distinct MYB, CEBPA, LYL1, SPI1, and RUNX1 DNA-binding motifs observed in CRYBMIM-treated cells (Figure 4A-B), associated with the apparent redistribution and remodeling of their CBP/P300 co-activator complexes (Figure 4C-D). Indeed, these factors directly associate with the MYB regulatory complex and their DNA binding motifs are enriched at loci affected by CRYBMIM treatment (Figure 4).

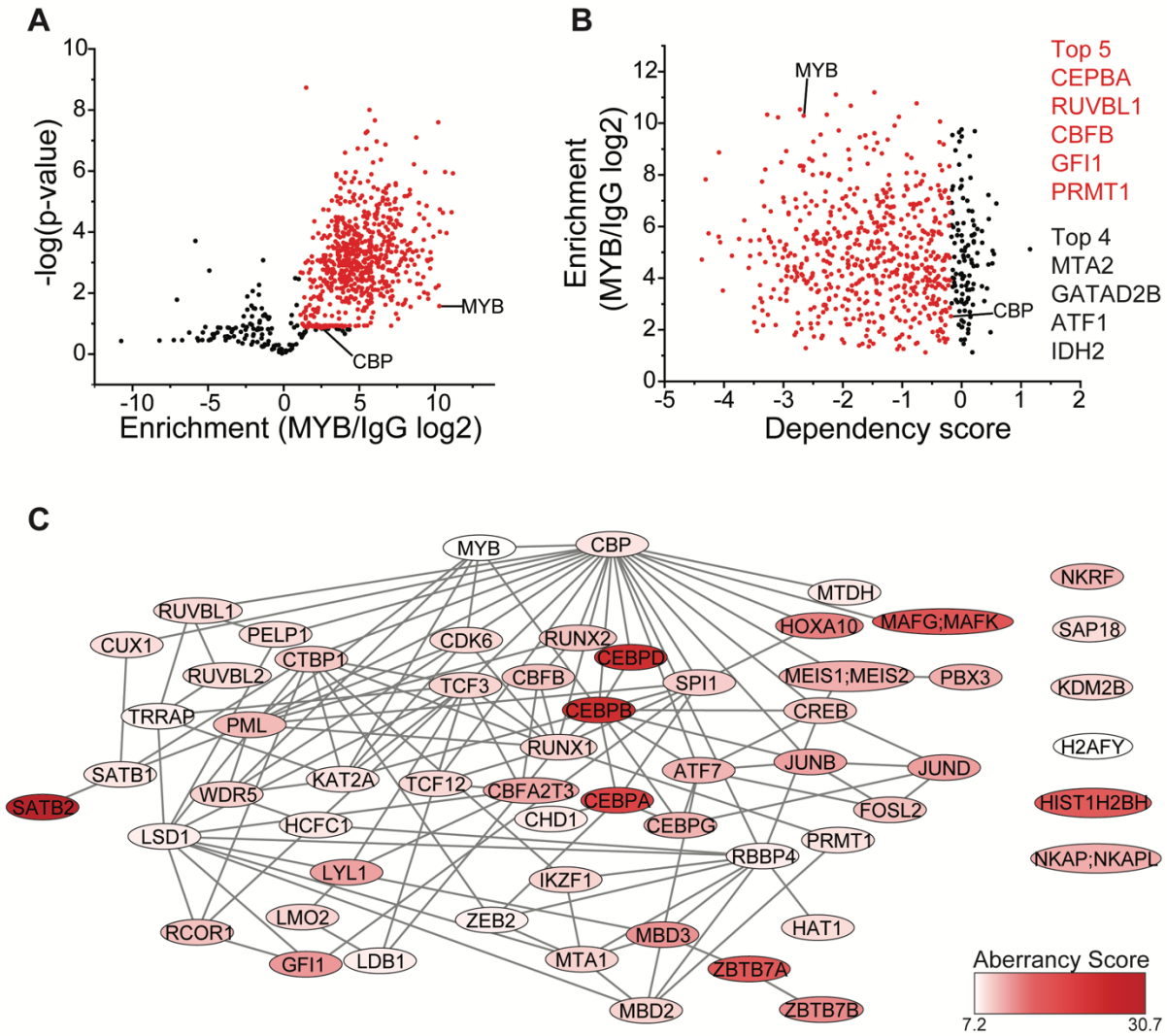

Release and redistribution of MYB-sequestered transcription factors restores normal myeloid differentiation

We reasoned that the remodeling of MYB regulatory complexes and their associated chromatin factors such as CBP/P300 are responsible for the anti-leukemia effects of CRYBMIM, at least in part via reactivation of cellular differentiation of MV411 AML cells (Figure 3). To test this, we prioritized CEBPA, LYL1, SPI1, and RUNX1 as MYB-associated co-factors based on their physical interactions and functional dependencies in AML cells (Figure 5), and analyzed their chromatin dynamics in response to CRYBMIM treatment using ChIP-seq analysis. Consistent with the release and redistribution mechanism, we observed both coherent and factor-specific dynamics of MYB co-factors on chromatin upon CRYBMIM treatment (Figure 6A). Clustering of observed dynamics revealed nine classes of apparent chromatin responses (Figure 6B). Approximately one third of the affected genes lost both MYB and CBP/P300 in response to CRYBMIM, as well as RUNX1, LYL1, and/or CEBPA (Figure 6B; yellow clusters 1, 3, and 6). Genes in the MYB and CBP/P300-depleted clusters 1, 3, and 6 were enriched in those associated with the development of hematopoietic progenitor cells, as well as MYC and HOXA9/MEIS1 targets (Table S6), consistent with current and past gene expression profiling studies (Figure 3). In addition, these genes were enriched in pathways involving chromatin repression, consistent with the enrichment of DNA-binding sequence motifs of transcriptional repressors YY1 and REST/NRSF (Figure 6B and Table S6). This suggests a potential mechanism for the long-hypothesized repressive functions of MYB. While we found no apparent changes in JUN occupancy, motif analysis at loci that both lost and gained MYB and CBP/P300 revealed enrichment of AP-1 sequence elements, consistent with the presence of other AP-1 family member(s) in MYB regulatory complexes. Minor apparent contribution of MYB:CBP/P300-independent chromatin dynamics involved genes enriched in MLL targets (Figure 6B, Tables S6; blue clusters 5, 8), consistent with the activity of MLL fusion proteins in MV411 cells.

Notably, the two chromatin dynamics clusters 4 and 9 that gained both MYB and CBP/P300 in response to CRYBMIM, associated with the accumulation of CEBPA, RUNX1, and/or CREB, were enriched in genes controlling myeloid differentiation programs (Figure 6B; orange, and Table S6). This is consistent with the CRYBMIM-induced gene expression differentiation programs and accompanying morphologic features of myeloid differentiation (Figure 3). It is possible that other transcription factors may contribute to oncogenic gene expression in AML cells, such as CREB for example, as evident from their contribution to MYB-independent chromatin dynamics (Figure 6B; pink cluster 2). However, this is likely a minor effect, given the relatively modest reprogramming of gene expression by CREBMIM that targets the CREB:CBP/P300 complexes in AML cells (Figure 2 and Figure S3).

These results support the model in which the core regulatory circuitry of AML cells is organized by MYB and its associated co-factors such as LYL1, CEBPA, SPI1, and RUNX1, which co-operate in the induction and maintenance of oncogenic gene expression. This involves apparent sequestration of CBP/P300 from genes controlling myeloid cell differentiation. Thus, oncogenic gene expression is associated with the assembly of aberrantly organized MYB transcriptional co-activator complexes, and their dynamic remodeling by selective blockade of protein interactions can induce AML cell differentiation.

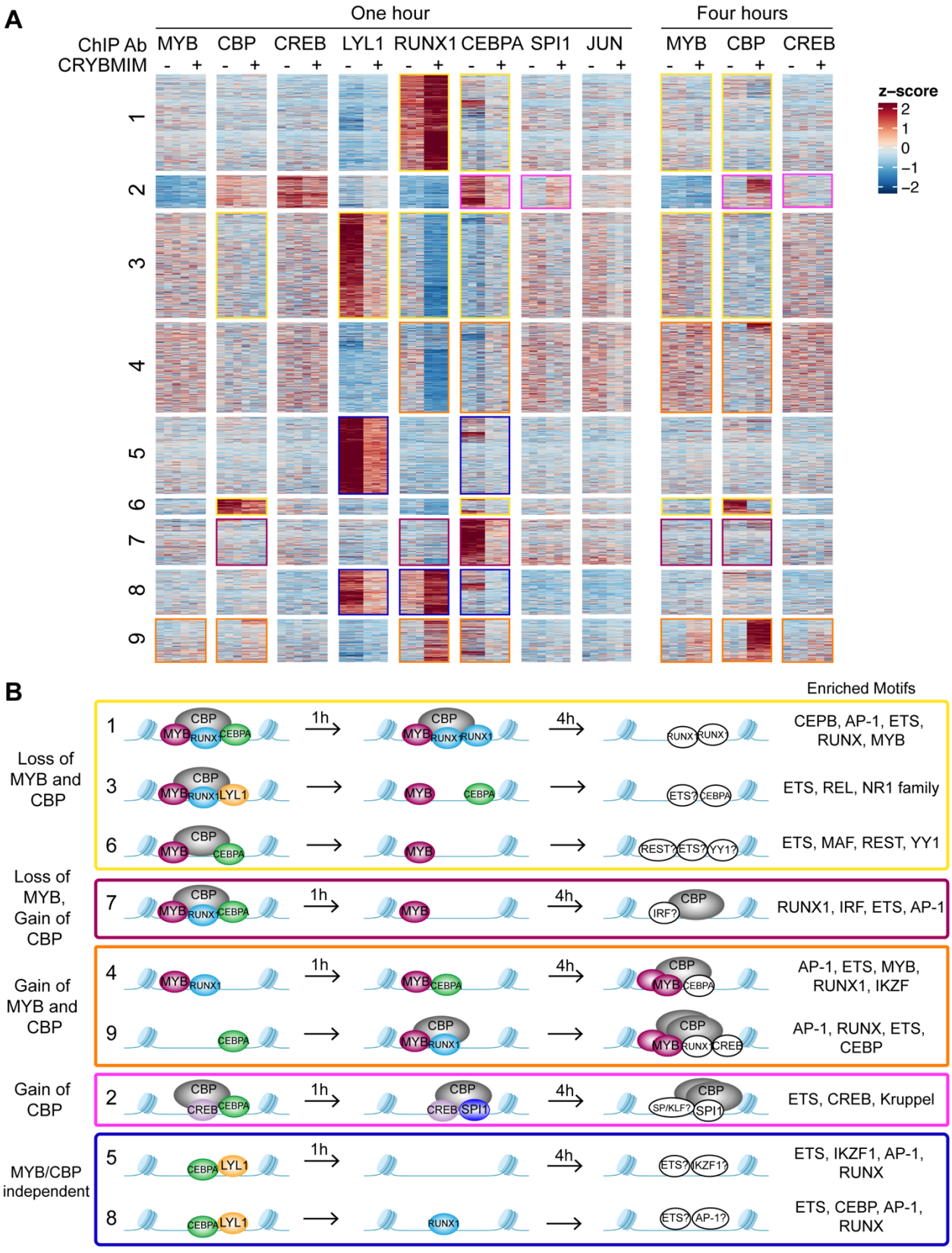

DISCUSSION

Dysregulated gene expression is a nearly universal feature of all human cancers. This is particularly relevant for leukemias which are frequently caused by mutations of genes encoding transcription and chromatin remodeling factors. Among all types of leukemias examined to date, the transcription factor MYB ranks as the most selectively required functional genetic dependency (Figure 1). This nominates MYB both as a compelling therapeutic target, and a focus of mechanistic studies to define fundamental mechanisms of dysregulated gene expression in leukemias.

By rapid and selective peptidomimetic interference with the binding of CBP/P300 to MYB, but not CREB or MLL (Figure 2), we find that the leukemic functions of MYB are mediated by CBP/P300-mediated co-activation of a distinct set of transcriptional factor complexes that are aberrantly assembled with MYB in AML cells. The second-generation, cell-penetrant peptidomimetic MYB inhibitor, termed CRYBMIM, has potent and broad-spectrum activity against diverse subtypes of AML, while sparing normal hematopoietic progenitor cells (Figure 2). Consequently, its improved activity enables high-resolution, genome-wide studies of chromatin and gene expression dynamics that control MYB-dependent leukemic expression in AML cells. We find that CRYBMIM blocks oncogenic MYB gene expression and restores myeloid cell differentiation (Figure 3). This effect involves aberrantly organized MYB regulatory complexes, composed of additional transcription factors including LYL1, CEBPA, SPI1 and RUNX1 (Figures 4 & 5), that are reminiscent of core regulatory circuits observed in MYB-dependent T-cell lymphoblastic leukemias and other cancers (Sanda *et al.*, 2012; Mansour *et al.*, 2014). Unexpectedly, we find that MYB-dependent leukemogenic gene expression also involves apparent sequestration of CBP/P300 (Figure 4 & 6). In turn, peptidomimetic MYB:CBP/P300 blockade releases and redistributes CBP/P300 and other sequestered transcription factors to induce cell differentiation (Figure 6). In all, these findings establish a compelling strategy for pharmacologic reprogramming of oncogenic gene expression that supports its targeting for leukemias and other human cancers caused by dysregulated gene control.

What is the origin of aberrant MYB functions in leukemia cells? MYB is not known to be mutated in most cases of AML, and this study points to its aberrant assembly as the convergent mechanism by which it is pathogenically dysregulated. Indeed, previous studies have found cell type-specific features of MYB gene activation, suggesting the presence of other factors that influence MYB activity (Lei *et al.*, 2004). Furthermore, MYB alone is not sufficient for leukemic cell transformation, indicating the need for specific co-factors in its leukemogenic activity (Gonda, Buckmaster and Ramsay, 1989; Hu *et al.*, 1991).

By integrating functional genomics and proteomics, combined with gene expression and chromatin dynamics mapping, we identified a set of factors in complex with MYB that appear to be aberrantly co-expressed, including CEBPA, LYL1, SPI1, and RUNX1. Their physical interactions and chromatin co-localization with MYB are associated with oncogenic gene expression and blockade of cell differentiation in AML cells. Interestingly, we found no CRYBMIM-induced remodeling of MYB regulatory complexes independent of CBP/P300, indicating that KIX-dependent interaction between MYB and CBP/P300 is required for all MYB transcriptional activity in AML cells.

It is possible that somatic mutations of regulatory DNA elements, such as those physically associated with MYB regulatory complexes (Figure 6), contribute to the aberrant assembly of these complexes on chromatin, as observed for the oncogenic *TAL1* enhancer mutations in cases of T-ALL (Mansour *et al.*, 2014), and recently suggested for other leukemias (He *et al.*, 2019). It is also possible that leukemic gene expression by MYB involves additional transcriptional co-activators, such as TAF12, as part of the recently described TFIID-SAGA complex interaction (Xu *et al.*, 2018), or other TAFs which have also been implicated in transcriptional co-regulation in leukemias (Jian *et al.*, 2017; Xu *et al.*, 2019). Lastly, it is also possible that distinct subtypes of

AML diverge from the aberrant regulatory complex assembly model presented here. For example, LYL1, an oncogene that is aberrantly expressed in diverse subtypes of AML (Meng *et al.*, 2005), assembles with MYB in leukemia cells examined in our study, similar to its functional homologue TAL1 in cases of T-ALL (Sanda *et al.*, 2012; Mansour *et al.*, 2014). Alternative bHLH transcription factors may cooperate with MYB in some leukemia subtypes (Jones, 2004). It will be important to determine how aberrant co-expression of such oncogenic regulatory complex co-factors is induced in leukemia cells, such as for example by kinase-dependent dysregulation of transcription factor assembly for MEF2C and LYL1 (Brown *et al.*, 2018; Tarumoto *et al.*, 2018; Vakoc and Kentsis, 2018). It will also be interesting to examine whether resistance of erythroblastic *BRC-ABL1*-translocated K562 cells to CRYBMIM represents a solitary case, or portends lack of dependence on MYB by *BCR-ABL1* fusion or erythroid leukemias.

The switch-like response of AML cells to peptidomimetic disassembly of the MYB:CBP/P300 chromatin complex suggests that cellular CBP/P300 exists in a dynamic equilibrium under limiting conditions. Such a model is supported by the Rubinstein-Taybi syndrome due to heterozygous deletion mutations of CBP that reduce CBP gene dosage, leading to human developmental defects. This model also explains the distinct requirements of CBP and P300 in normal hematopoiesis and leukemia cell development (Wang *et al.*, 2011; Cheng *et al.*, 2017), as well as the functional requirement for P300 in CBP-deficient cancers (Ogiwara *et al.*, 2016). Definition of the mechanisms of this molecular switch regulating discrete gene expression programs is expected to reveal distinct mechanisms of dysregulated gene control in AML and other transcription-dysregulated cancers.

Current small molecule inhibitors of MYB lack sufficient selectivity (Pattabiraman and Gonda, 2013; Uttarkar *et al.*, 2015, 2016). Our peptidomimetic strategy suggests that structure-based design of effective pharmacologic MYB inhibitors is not only possible, but also desirable given its favorable therapeutic index. First, the functional requirement for peptidomimetic blockade of MYB but not CREB or MLL binding in supporting oncogenic gene expression and cell survival suggests that ligands to these permissive binding sites may be used to gain binding affinity of pharmacologic MYB inhibitors. Indeed, such a fragment-based design strategy was successfully used to develop effective BH3 mimetics, including venetoclax that has recently been approved for leukemia therapy. Similarly, functional proteomic maps of MYB regulatory complexes provided by our study should be useful in identifying key protein-protein interactions and post-translational enzymatic modifications that are aberrantly induced in AML cells, as targets for improved therapies. For example, this may involve transcription factor acetylation by CBP/P300 (Wang *et al.*, 2011; Roe *et al.*, 2015), warranting the investigation of recently developed selective CBP/P300 acetyltransferase inhibitors, which have shown particular activity in hematopoietic cancers (Lasko *et al.*, 2017).

Recent studies have found that stable non-genetic resistance is a common feature of relapsed AML, and this resistance at least in part is due to the use of alternative enhancers to sustain aberrant gene expression (Bell *et al.*, 2019). Therapeutic remodeling of complexes of master regulators such as MYB may constitute an effective strategy to reprogram oncogenic gene expression that may prevent or overcome such resistance, providing a platform for therapy of regulatory complex-mediated gene dysregulation in human cancers. Development and investigation of clinical-grade MYB inhibitors, including improved derivatives of MYBMIM and CRYBMIM, are important directions of future work for patients with MYB-dependent acute myeloid and lymphoblastic leukemias, blastic plasmacytoid dendritic cell neoplasms, gliomas, breast, colon and adenoid cystic carcinomas.

METHODS

Reagents

Synthetic peptides were produced by solid phase synthesis, purified by liquid chromatography, and confirmed by mass spectrometry (Tufts University Core Facility). Peptides were dissolved in phosphate buffered saline (PBS) at a concentration of 1 mM, as measured using optical absorbance measurements at 280 nm and extinction coefficients. Cell culture media was obtained from Corning. All cell lysis buffers were supplemented with a protease inhibitor mix comprised of AEBSF (0.5 mM, Santa Cruz, SC-202041B), bestatin (0.01 mM, Fisher/Alfa Aesar, J61106-MD), leupeptin (0.1 mM, Santa Cruz, SC-295358B), and pepstatin (0.001 mM, Santa Cruz, SC-45036A).

Cell culture

The cell lines MV-411, MOLM-13, OCIAML2, THP1, NB4, KASUMI1, HEL, OCIAML3, SKM1, U937, HL-60, and K562 were obtained from the American Type Culture Collection (ATCC, Manassas, Virginia, USA). The identity of all cell lines was verified by STR analysis (Integrated Genomics Operation Core Facility, MSKCC) and absence of Mycoplasma contamination was determined using Lonza MycoAlert (Lonza Walkersville, Inc., Walkersville, MD, USA). Cell lines were cultured in 5% CO_2 in a humidified atmosphere at 37˚ C and were maintained in RPMI 1640 medium supplemented with 10% fetal bovine serum (FBS) (VWR), antibiotics (100 U/ml penicillin and 100 μg/mL streptomycin), and L-glutamine (1%). Umbilical cord human blood was obtained from the New York Blood Center.

Peptide KIX molecular structures

All structures were built in Maestro (Schrodinger). Structures of KIX with MYB, CREB, and MLL peptides were modeled based on PDB IDs 1SBO, 1KDX, and 2LSX, respectively. For CRYBMIM, PDB 1KDX was used as a starting model, replacing CREB amino acids 137-146 with MYB amino acids 298-310. Resulting models were energy minimized using MacroModel (Schrodinger) using the OPLS_2005 force field with implicit water at a dielectric constant of 80.

Expression and purification of recombinant CBP KIX domain

CBP KIX was purified as described previously (Ramaswamy *et al.*, 2018). BL21(DE3) cells (Invitrogen) transformed with pGEX-KIX plasmid were induced at 37° C with isopropyl beta-D-1-thiogalactopyranoside (IPTG) for 3 hours. Cells were harvested by centrifugation at 3000 x g for 15 min. Pellets were resuspended in lysis buffer of 50 mM Tris-HCl pH 7.3, 150 mM NaCl, 0.1% Tween-20, 1 mM DTT, 5 mM EDTA, supplemented with protease inhibitors at a ratio of 50 mL lysis buffer per 1 L of bacterial culture. Cells were lysed for ten minutes on ice (15 sec on, 15 sec off, 40% amplitude) using the Misonix probe sonicator (Qsonica, Newtown, CT). Lysates were cleared by centrifugation for 1 h at 21,800 x g at 4° C. Cleared lysates were incubated with 4 mL glutathione agarose resin slurry (GoldBio) for 1 h at 4° C to capture GST-KIX. Resin was washed four times with 50 mM Tris-HCl pH 7.4, 150 mM NaCl. KIX domain was cleaved from GST by incubation of resin-bound GST-KIX with 160 U thrombin (GE Healthcare) overnight at room temperature. Resin was centrifuged at 500 x g for 5 min. Supernatant containing cleaved KIX was collected and dialyzed at 4° C against 1 L of 50 mM MOPS pH 6.5, 50 mM NaCl, 10% glycerol, 1 μM tris-2-carboxyethylphosphine (TCEP) overnight at 4˚ C with mixing. Cleaved KIX was purified using a linear gradient of 50 mM to 1 M NaCl over ten column volumes by cation exchange chromatography using MonoS 5/50 GL column at a flow rate of 1 mL per minute (GE Healthcare). Fractions containing purified KIX were confirmed by SDS-PAGE and dialyzed against 1 L of 50

mM potassium phosphate pH 5.5, 150 mM NaCl, 10 μM TCEP, 30% glycerol overnight at 4˚ C with mixing. Purified protein was aliquoted and stored at -80° C.

Microscale thermophoresis (MST)

Binding of purified recombinant KIX with fluorescein isothiocyanate (FITC)-conjugated peptides was measured by microscale thermopheresis using the Monolith NT.115 (NanoTemper Technologies). Assays were conducted in 50 mM sodium phosphate, 150 mM NaCl, 0.01% NP-40, pH 5.5. FITC-conjugated peptides (FITC-CREBMIM at 300 nM, FITC-CRYBMIM at 250 nM, and FITC-MYBMIM at 2000 nM, as based on the optical absorbance measurements of FITC at 495 nm) were mixed with increasing concentrations of purified KIX (0.0015 to 50 μM, 1:1 serial dilutions) and loaded into MST Premium Coated capillaries. MST measurements were recorded at room temperature for 10 sec per capillary using fixed IR-laser power of 80% and LED excitation power of 40-50%.

Confocal microscopy

Confocal imaging was performed using the Zeiss LSM880 confocal microscope and 63X objective with 1.5 micron z-stack images. Nunc Lab-tek II 8-chamber coverslips were prepared for cell adhesion by the addition of poly-L-Lysine and incubation at room temperature for 1 h. Poly-L-lysine solution was removed from each chamber and chambers were allowed to air dry. 2 x 10^5 cells in 200 μL of fresh media were added to each chamber and incubated for 1 hour at 37° C for attachment. FITC-conjugated peptides were added to cell suspensions at a concentration of 100 nM, mixed, and incubated for 1 hour at 37° C. Cells were counter-stained using Hoechst 33342 and Mitotracker Red CMX ROS (MProbes) for 10 minutes at a final dilution of 1:10,000 prior to imaging.

Blood progenitor colony forming assays

Mononuclear cells were isolated from cord blood using Ficoll-Paque PLUS density centrifugation and enriched for $CD34^+$ cells using the CD34 MicroBead Kit UltraPure, according to the manufacturer's instructions (Miltenyi Biotech). $CD34^+$ cells were resuspended to a concentration of $1x10^5$ cells/mL. Methocult H4034 Optimum (Stemcell Technologies, Catalog no. 04034 with FBS, BSA and recombinant human SCF, GM-CSF, G-CSF, IL-3, and erythropoietin) semi-solid media was used for the growth of hematopoietic progenitor cells in colony-forming units. Methocult and CD34+ cells were mixed in a ratio of 1:10 (cells:Methocult) for a final cell concentration of 1000 cells/dish. Peptides were added to this solution for a final concentration of 20 μM each. Mixture was vortexed for 30 seconds and incubated at room temperature for 5 minutes. Using a blunt-end 18 G needle, 1.1 mL of the solution was added to each 35 x 10 mm dish and then tilted to cover. Peptide treatment conditions were analyzed in biological triplicates. 35 x 10 mm dishes were placed into a larger 100 x 15 mm dish with one 35 x 10 mm dish filled with sterile water. Dishes were incubated at 37° C with 5% CO2 for 14 days. Both erythroid progenitor and granulocyte-macrophage progenitors were observed and quantified. Brightfield microscopy CFU-GM and BFU-E colony images were obtained using 10X and 20X magnification on the Zeiss Axio Observer microscope.

Cell viability analysis

Cells were resuspended in fresh media and plated at a concentration of $2x10^5$ cells in 200 μL per well in a 96-well plate. Peptides or PBS control were added at indicated concentrations. Cells were incubated at 37° C with 5% CO2 for 6 days with media and peptide replacement every

48 hours. On day 6, cell viability was assessed using the CellTiter-Glo Luminescent Viability assay, according to the manufacturer's instructions (Pscfromega). Luminescence was recorded using the Infinite M1000Pro plate reader with an integration time of 250 milliseconds (Tecan). For dose-response assays, cells were resuspended and plated at a concentration of 2000 cells in 200 μL per well of a 96-well plate. MV411 cells were plated in complete RPMI media described above. CD34+ cells isolated from umbilical cord blood were plated in Iscove's Modified Dulbecco's Medium (IMDM) media supplemented with 15% FBS, 100 U/mL penicillin and 100 μg/mL streptomycin, 1% L-glutamine, recombinant human cytokines (PeproTech: 100 ng/mL SCF, 100 ng/mL TPO, 100 ng/mL FLT3, 20 ng/mL IL-6, 20 ng/mL IL-3), and 50 μM β-mercaptoethanol. Increasing concentrations of peptides (0.78 to 100 μM; 1:1 serial dilution) were added as indicated. Cells were incubated for 48 hours at 37° C with 5% CO_2. Cell viability was assessed using Cell Titer Glo as described above.

Western blot analysis

Cells were lysed in directly in Western blot sample buffer (30 mM Tris-HCl pH 6.8, 1% SDS, 2% beta-mercaptoethanol, 7% glycerol, 0.0002% Bromophenol Blue) supplemented with protease inhibitors at a ratio of 200 μL sample buffer per 1 million cells. Cell suspensions were incubated at 95° C for 15 min, with vortexing every 5 min. Lysates were clarified by centrifugation for 5 min at 18,000 x g. Twenty μL of clarified lysates were resolved by sodium dodecyl sulfate-polyacrylamide gel electrophoresis (SDS-PAGE) using 10% polyacrylamide Bis-Tris gels (Invitrogen) and transferred onto Immobilon FL PVDF membranes at 30V for 90 min (Millipore, Billerica, MA, USA). Membranes were blocked using Odyssey Blocking buffer (Li-Cor, Lincoln, Nebraska, USA). Blots were incubated in primary antibodies as indicated. Blotted membranes were visualized using secondary antibodies conjugated to IRDye 800CW or IRDye 680RD (goat anti-rabbit, 1:15,000, and goat anti-mouse, 1:15,000) and the Odyssey CLx fluorescence scanner, according to manufacturer's instructions (Li-Cor, Lincoln, Nebraska, USA).

Nuclei isolation from AML cells

Nuclear purifications were carried out per 100 million cells. Cells were collected by centrifugation at 400 x g for 5 min and washed in cold PBS. Washed cell pellets were resuspended in 15 mL hypotonic buffer (10 mM HEPES pH 7.9, 10 mM NaCl, 1 mM $MgCl_2$, 0.5 mM DTT, protease inhibitors) and incubated on ice for 1 hour. Cells were lysed using 40 strokes by Dounce homogenization. Suspensions were then centrifuged for 15 min at 3000 x g to pellet nuclei. Nuclear pellets were further purified by sucrose density gradient centrifugation. Pellets were resuspended in 2.5 mL of 0.025 M Sucrose, 10 mM $MgCl_2$ and layered on top of 2.5 mL 0.88 M sucrose, 0.05 mM $MgCl_2$ and centrifuged for 10 min at 1200 x g. The final nuclear pellet was resuspended in 1 mL lysis buffer (50 mM Tris-HCl pH 7.4, 150 mM NaCl, 0.25 mM EDTA, 1 mM DTT, 0.5% Triton X-100, 10% glycerol, protease inhibitors) and incubated on ice for 20 min. Nuclear suspensions were homogenized by 15 strokes in a Dounce homogenizer without frothing, and clarified by centrifugation for 15 min at 18,000 x g. Clarified lysates were diluted to a total of 4 mL lysis buffer and immediately used for immunoprecipitations.

Co-immunoprecipitation

For MYB immunoprecipitations, 7.5 μg of anti-MYB antibodies (EP769Y, Abcam) were conjugated to 1 mg of M-270 Epoxy-coated magnetic beads (Invitrogen) according to manufacturer's instructions. For CBP immunoprecipitations, 50 μL of each of Protein A and Protein G Dynabeads (Invitrogen) were combined and washed in 1 mL of PBS with 0.5% BSA.

Fifteen μg of anti-CBP antibodies were added to Protein A/G beads in 1 mL PBS with 0.5% BSA and incubated for 1 h at room temperature with rotation. Beads were then washed with 1 mL PBS with 0.5% BSA and beads were resuspended in a final volume of 100 μL of PBS with 0.5% BSA. One hundred million cells were used per immunoprecipitation. For displacement assays, cells were treated with 10 μM peptides as indicated for 1 hour at 37° C in complete RPMI media prior to nuclei isolation. Immunoprecipitations were carried out using 100 μL of respective antibody-bead slurry per immunoprecipitation overnight at 4° C with rotation. Beads were washed 3 times with 1 mL of cold lysis buffer. Proteins were eluted in 40 μL of 0.2 M glycine pH 3 for 30 min on a ThermoMixer (Eppendorf) at 900 rpm. Eluates were neutralized with 2 μL of 1 M Tris pH 11. Samples were prepared for Western blot by addition of Western blot sample buffer described above and incubated at 95° C for 5 min. Presence of various proteins was assessed by Western blot as described.

Streptavidin affinity purification

Streptavidin magnetic beads (Pierce) were washed with 30 mM Tris-HCl pH 7.4, 150 mM NaCl, 0.1% Tween-20 (TBST) twice prior to use. For each purification, 100 μL of streptavidin beads were used (1 mg beads, binding capacity 3500 pmol biotinylated fluorescein per mg). Biotinylated peptides were bound to streptavidin bead slurry by incubation at room temperature for 1 h in TBST. Peptide-bound beads were washed twice in TBST and immediately used for purifications. Nuclear lysates were extracted as described above for co-immunoprecipitation. Twenty million cells were used per purification. Nuclear lysates were incubated with Bio-CREBMIM or Bio-CRYBMIM as indicated for 1 h at room temperature with rotation. Beads were washed twice in lysis buffer and separated for subsequent competition. Per competition, beads were incubated in a total of 1 mL of lysis buffer supplemented with competing peptide for 1 h at room temperature with rotation. Beads were washed twice in lysis buffer. Bound proteins were eluted by adding 40 μL of Western blot sample buffer described above and incubated for 20 min at 95° C, with vortexing half way through. Presence of CBP/P300 was assessed by Western blot as described.

Quantitative RT-PCR

Cells were treated as described above for cell viability assays for indicated times points. RNA was isolated using RNeasy kit according to the manufacturer's instructions (Qiagen). Complementary DNA was synthesized using the SuperScript III First-Strand Synthesis system according to the manufacturer's instructions (Invitrogen). Quantitative real-time PCR was performed using the KAPA SYBR FAST PCR polymerase with 200 ng template and 200 nM primers, according to the manufacturer's instructions (Kapa Biosystems, Wilmington, MA, USA). Ct values were calculated by ROX normalization using the ViiA 7 software (Applied Biosystems).

Chromatin immunoprecipitation and sequencing (ChIP-seq)

To prepare antibody-coupled beads, 30 μg of antibodies as indicated per ChIP were incubated with 1 mg of 1:1 Protein A/Protein G slurry in PBS with 0.5% BSA overnight at 4° C with rotation. Beads were washed twice in PBS with 0.5%. Fifty million cells were used per ChIP assay. Cells were fixed in 1% formaldehyde for 10 minutes at room temperature. Crosslinking was quenched by adding glycine to a final concentration of 125 mM and incubating at room temperature for 5 min. Cells were pelleted by centrifugation at 500 x g at 4° C for 5 min. Cells were washed twice by resuspending 5 mL of PBS with 1 mM PMSF and centrifuging at 500 x g at 4° C for 5 min. Wash step was repeated twice. Crosslinked pellets were resuspended in 2 mL of 50 mM Tris-HCl pH 8.1, 100 mM NaCl, 5 mM EDTA, 0.2% NaN_3, 0.5% SDS, and protease

inhibitors. Nuclei were pelleted by centrifugation at 15,000 x g for 10 min at 4° C. Pellets were resuspended in 50 mM Tris-HCl, 100 mM NaCl, 5 mM EDTA, 0.2% NaN_3, 0.3% SDS, 1.5% Triton X-100, and protease inhibitors and sonicated using the Covaris S220 adaptive focused sonicator at 5% duty Factor, 140W peak incident power, 200 cycles per burst for 30 min at 4° C to obtain 100-500 base pair chromatin fragments (Covaris, Woburn, CA). Nuclear sheared lysates were clarified by centrifugation at 15,000 x g for 10 min at 4° C. Supernatants were incubated with antibody-coupled Protein A/G beads as indicated overnight at 4° C with rotation. Beads were washed 3 times in 1 mL of 50 mM HEPES-KOH pH 7.6, 500 mM LiCl, 1 mM EDTA, 1% NP-40, 0.7% Na deoxycholate. For the final wash, 1 mL of 50 mM Tris-HCl pH 8, 10 mM EDTA, 50 mM NaCl was added to the beads. Beads were centrifuged for 3 min at 960 x g at 4° C and supernatant was removed. To elute, 210 μL of 50 mM Tris-HCl pH 8, 10 mM EDTA, 1% SDS was added to the beads and incubated for 30 min at 65° C. Beads were centrifuged for 1 min at 16,000 x g at room temperature. Supernatant contains eluted samples. Crosslinks were reversed by incubation overnight at 65° C. Samples were diluted to 400 μL with 50 mM Tris-HCl pH 8, 10 mM EDTA, 50 mM NaCl, and 4 μL of 500 ug/ml RNase (Roche, Cat. No 11119915001) was added and incubated for 1 h at 37° C to digest RNA. Proteins were then digested by addition of 2 μL 20 mg/mL Proteinase K (Roche, Cat. No. 03115828001) and incubation for 2 h at 55° C. Samples were purified using PureLink PCR Purification Kit. Libraries were prepared using the NEBNext ChIP-seq library prep kit (New England Biolabs), according to the manufacturer's instructions, and sequenced on the Illumina HiSeq 2500 instruments, with 20-30 million of 50-bp paired-end reads for each sample.

For ChIP-seq analysis, reads were quality and adapter trimmed using 'trim_galore' before aligning to human genome assembly hg19 with bowtie2 using the default parameters. Aligned reads with the same start position and orientation were collapsed to a single read before subsequent analysis. Density profiles were created by extending each read to the average library fragment size and then computing density using the BEDTools suite. Enriched regions were identified using MACS 2.0 and scored against matched input libraries. Genomic 'blacklisted' regions were filtered (http://www.broadinstitute.org/~anshul/projects/encode/rawdata/blacklists/hg19-blacklist-README.pdf) and remaining peaks within 500 bp were merged. Read density normalized by sequencing depth was then calculated for the union of peaks, and peak dynamics were assessed in DESeq2 using a fold change of 1.5 and an FDR-adjusted p-value of 0.05.

RNA sequencing (RNA-seq)

Cells were treated with peptide or control as described above for cell viability assays at 20 μM for 1 hour and 4 hours. Cells were collected and RNA was isolated using RNeasy kit (Qiagen) according to manufacturer's instructions. Reads were quality and adapter trimmed using 'trim_galore' before aligning to human assembly hg19 with STAR v2.5 using the default parameters. Coverage and post-alignment quality were assessed using the Picard tool CollectRNASeqMetrics (http://broadinstitute.github.io/picard/). Read count tables were created using HTSeq v0.6.1. Normalization and expression dynamics were evaluated with DESeq2 using the default parameters.

Flow cytometric analysis of apoptosis and differentiation

MV411 cells were resuspended to a concentration of $1x10^6$ cells per mL and plated in 12-well tissue culture plates. To assess apoptosis, MYBMIM was used as a positive control and cells were treated as described (Ramaswamy *et al.*, 2018). Cells were treated with 20 μM CRYBMIM for one hour. Following peptide treatment, cells were washed with PBS and resuspended with

PBS with the addition of Annexin V-FITC (1:50) and CD11b (1:50). Cells were incubated on ice for 40 minutes followed by two washes with cold PBS. DAPI was added prior to flow cytometric analysis (1:10,000).

Gene dependency analysis across cancer cell types

CRISPR knockout screen gene effect data from Project Achilles 19Q4 was downloaded from the DepMap Consortium (DepMap, Broad (2019): DepMap 19Q4 Public Dataset doi:10.6084/m9.figshare.11384241.v2). Dependency scores for each gene were averaged by tumor type. A differential dependency score was then calculated as the relative difference between the average gene dependency score for a tumor type and the average gene dependency score across all cell types. All genes were then ranked by leukemia gene differential dependency scores, and the top 10 and bottom 10 leukemia gene dependencies were plotted as a heat map. P-values were calculated comparing MYB dependency in leukemias versus all other tumor types using two-tailed t-test.

In-gel digestion and Mass Spectrometry analysis

Immunoprecipitations were carried out as described above in biological triplicates. Eluates were resolved by SDS-PAGE 10% polyacrylamide Bis-Tris gels (Invitrogen) at 100 V for 5 minutes. To visualize proteins, gels were stained using Silver Stain for Mass Spectrometry kit (Pierce) according to manufacturer's instructions. Relevant gel portions were excised and destained using 50 μL of 30 mM $K_3[Fe(CN)_6]$ in 100 mM aqueous $Na_2S_2O_3$ by incubation at room temperature for 30 minutes, with gentle mixing halfway through. Following destaining, 500 μL of 25 mM aqueous NH_4HCO_3 were added to each tube and incubated for 5 min at room temperature on a ThermoMixer (Eppendorf) at 700 rpm. Solution was removed and gel pieces were washed by adding 500 μL of 50% acetonitrile in 25 mM aqueous NH_4HCO_3 and incubating for 10 min at room temperature on a ThermoMixer at 700 rpm. Wash step was repeated 2 more times. All solution was removed and 100 μL of acetonitrile was added to each tube and incubated for 5 min at room temperature on a ThermoMixer (Eppendorf) at 700 rpm. All solution was removed and destained gel fragments were vacuum centrifuged and stored at -20C. For reduction of disulfide bonds, gel fragments were re-hydrated in 25 μL of 10 mM dithiothreitol in 100 mM aqueous NH_4HCO_3 for 1 h at 56C. Tubes were cooled to room temperature. For alkylation of thiols, 25 μL of 55 mM iodoacetamide in 100 mM aqueous NH_4HCO_3 was added to each tube and incubated for 30 min at room temperature in the dark. To quench the alkylation reaction, 5 μL of 100 mM dthiothreitol in 100 mM aqueous NH_4HCO_3 was added and incubated for 5 min at room temperature. Gel fragments were washed by adding 50 μL of acetonitrile and incubation for 5 min at room temperature followed by addition of 500 μL of 100 mM aqueous NH_4HCO_3 and incubation for 10 min at room temperature. All solution was removed and wash step was repeated. All solution was removed and 100 μL of acetonitrile was added and tubes were incubated for 10 min at room temperature. All solution was removed and gel fragments were vacuum centrifuged and stored at -20C. For digestion of proteins into peptides, gel fragments were cooled on ice. Protease LysC was added at a ratio of 1:25 protease:protein, assuming 1 μg of protein per immunoprecipitation. Gel fragments were incubated for 5 min on ice. Samples were diluted to 50 μL, or to cover gel fragments using 50 mM aqueous NH_4HCO_3. Digestion was carried out for 4 hours at 37C. Following LysC digestion, trypsin was added to each tube at the 1:25 protease:protein ratio in 50 mM aqueous NH_4HCO_3. Trypsin digestion was carried out for 16 hours at 37C. To elute peptides from gel fragments, 50 μL of 1% formic acid in 70% acetonitrile was added to each tube and incubated for 30 min at room temperature on a ThermoMixer at 1400 rpm. Eluates were removed and saved, and elution step was repeated with fresh 1% formic acid

in 70% acetonitrile. New eluates were pooled with the first elution for a total of 100 μL of eluate per sample. Samples were vacuum centrifuged to dryness. Prior to mass spectrometry analysis, samples were desalted and purified by solid phase extraction using C18 Micro SpinColumns (Nest Group) and eluted with 70% acetonitrile supplemented with 0.1% formic acid. Eluates were vacuum centrifuged to remove all solution. Samples were resuspended in 8 μL of 0.1% aqueous formic acid and sonicated for 5 minutes to ensure full resuspension. Three μL of each sample were used for mass spectrometry analysis.

The LC system used a vented trap-elute configuration (EasynLC1000, Thermo Fisher scientific) coupled to an Orbitrap Lumos mass spectrometer (Thermo Fisher Scientific, San Jose, CA) via a nano electro-spray DPV-565 PicoView ion source (New Objective). The trap column was fabricated with a 5 cm × 150 μm internal diameter silica capillary with a 2 mm silicate frit, and pressure loaded with Poros R2-C18 10 μm particles (Life Technologies). The analytical column consisted of a 25 cm × 75 μm internal diameter column with an integrated electrospray emitter (New Objective), packed with ReproSil-Pur C18-AQ 1.9 μm particles (Dr. Maisch). Peptides were resolved over 90 min using a 3%-45% gradient of acetonitrile with 0.1% aqueous formic acid at 250 nL/minute.

Precursor ions in the 375–3000 m/z range were isolated using the quadrupole and recorded every 3 s using the Orbitrap detector (60,000 resolution, with 445.1200 ions used as lockmass), with an automatic gain control target set at 10^6 ions and a maximum injection time of 50 ms. Data-dependent precursor ion selection was enforced, limiting fragmentation to monoisotopic ions with charge 2–5 and precursor ion intensity greater than $5x10^4$, and dynamically excluding already fragmented ions for 30 s (10 ppm tolerance). Selected ions were isolated (Q1 isolation window 0.7 Th) and fragmented using HCD (normalized collision energy 30) using the top speed algorithm. Product ion spectra were recorded in the Orbitrap at 30,000 resolution (AGC of $8x10^4$ ions, maximum injection time 54 ms), in profile mode.

Mass spectra were analyzed using MaxQuant (version 1.6.0.16). For identification, spectra were matched against the human UniProt database (as of October 2017), supplemented with contaminant proteins from the cRAP database with FDR <0.01. After m/z recalibration, mass tolerance was set at 4.5 and 20 ppm for precursor and fragment ions, respectively. Cysteine carbamidomethylation was set as fixed chemical modification, while methionine oxidation and protein N-terminus acetylation were set as variable. Protease specificity was set to trypsin/P, with up to two missed cleavages allowed. The match between runs feature was enabled (0.7 min tolerance, 20 min alignment). Quantification was performed using the LFQ algorithm.

Contaminating peptides such as keratin and non-human proteins were excluded and label-free quantification (LFQ) intensity values for protein groups were used for analysis. IgG and MYB immunoprecipitation samples were analyzed together (3 replicates per condition; 6 samples total). Proteins in the following categories were excluded from analysis: (i) zero LFQ intensity across all replicates, (ii) zero LFQ intensity in 5 of 6 replicates, (iii) proteins with LFQ intensity recorded in only 1 replicate in both sets of samples. Enrichment scores were defined as the log2 ratio of MYB:IgG.

SUPPLEMENTAL INFORMATION

All supplemental data and files are available openly via Zenodo (https://doi.org/10.5281/zenodo.3780648). Raw mass spectrometry proteomics data are available via PRIDE. Raw gene expression and chromatin dynamics data are available via Gene Expression Omnibus.

ACKNOWLEDGEMENTS

We thank Alejandro Gutierrez, Marc Mansour, and Kristian Helin for critical comments on the manuscript. We thank Henrik Molina, Caitlin Steckler, and the MSK Integrated Genomics Operation core for technical assistance. This research was supported by the NIH R01 CA204396, T32 GM073546, P30 CA008748, St. Baldrick's Foundation, Hyundai Hope on Wheels, Burroughs Wellcome Fund, Damon Runyon-Richard Lumsden Foundation, Rita Allen Foundation, Leukemia & Lymphoma Society, the Starr Cancer Consortium, and Mr. William H. and Mrs. Alice Goodwin and the Commonwealth Foundation for Cancer Research and the Center for Experimental Therapeutics at MSKCC.

AUTHOR CONTRIBUTIONS

Conceptualization, LF and AK; Investigation, LF, PC, GM, CC, ST; Analysis, LF, PC, ST, RK, AK Resources, MK, AK; Writing of original draft, LF and AK; Writing of final draft, all authors; Funding acquisition, AK, MK.

DECLARATION OF INTERESTS

A patent application related to this work has been submitted to the U.S. Patent and Trademark Office entitled ''Agents and methods for treating CREB binding protein-dependent cancers'' (application PCT/US2017/059579).

FIGURE LEGENDS

Figure 1. CRYBMIM is an improved peptidomimetic chimera that specifically binds the KIX domain of CBP/P300 in vitro and in cells.
(A) Heatmap of the top 10 and bottom 10 gene dependencies for survival and proliferation of 652 cancer cell lines in the DepMap Cancer Dependency Map Project, ranked by the greatest dependency for 37 leukemia lines, 20 of which are AML cell lines, as indicated by the red color gradient; * p = 1.1e-15, t-test of leukemia versus other tumor types.
(B) Retro-inverso amino acid sequences of MYBMIM, CREBMIM and CRYBMIM, with amino acids derived from MYB, CREB, and TAT marked in blue, green, and black, respectively.
(B) Molecular model of the CRYBMIM:KIX complex. Residues making contact with KIX are labeled, with portions derived from MYB and CREB marked in blue and green, respectively.
(D) Binding of FITC-conjugated CREBMIM (blue), CRYBMIM (red), and MYBMIM (black), as measured using microscale thermophoresis; K_d = 2.9 ± 0.7, 5.7 ± 0.2, and 17.3 ± 1.6, respectively. Error bars represent standard deviations of three biological replicates; p < 1e-15, ANOVA, for CRYBMIM versus MYBMIM.
(E) Western blot showing binding of nuclear CBP/P300 isolated from AML cells to biotinylated CRYBMIM or CREBMIM, specifically competed by the excess free peptides as indicated.
(F) Quantification of CBP/P300 binding to CRYBMIM and CREBMIM by fluorescence densitometry, with black, gray and red denoting PBS control, TAT control, and peptide competition, respectively.

Figure 2. Potent and broad-spectrum activity of CRYBMIM against diverse AML cell lines.
(A) Representative live cell confocal microscopy images of MV411 cells treated with 100 nM FITC-conjugated peptides as indicated for 1 hour, counterstained with Mitotracker (red) and Hoechst 33342 (blue). Scale bar indicates 20 μm, with z-stack of 1.5 μm.
(B) Western blots showing immunoprecipitated nuclear CBP/P300 co-purified with MYB and CREB from MV411 cells treated with 10 μM peptides as indicated for 1 hour.
(C-E) Cell viability of MV411 cells as a function of increasing concentrations of 48-hour peptide treatment, comparing (C) CRYBMIM to CREBMIM and MLLMIM (IC_{50} = 6.88 ± 3.39, 29.15 ± 3.79, and 24.22 ± 2.00, p < 1e-15, ANOVA); (D) TG3 and CG3 (IC_{50} = 16.65 ± 1.00 and 48.91 ± 2.55, p <1e-15, ANOVA); and (E) CRYBMIM effect on MV411 as compared to normal CD34+ cells isolated from human umbilical cord blood (IC_{50} = 12.78 ± 3.63, p = 1.05e-15, ANOVA). Error bars represent standard deviation of three biological replicates.
(F) Cell viability of AML cell lines treated with control PBS (black), 20 μM CREBMIM (blue), MYBMIM (gray), or CRYBMIM (red) as indicated for 6 days with media replacement every 48 hours in three biological replicates (CRYBMIM versus control, p = 8.62e-3, t-test).

Figure 3. CRYBMIM blocks oncogenic MYB gene expression and restores normal myeloid cell differentiation.
(A-B) Volcano plots of normalized gene expression of one hour (A) and four hour (B) CRYBMIM-treated cells, as compared to control, with select genes labeled; p-values denote statistical significance of 3 biological replicates.
(C-E) Gene set enrichment analysis of up- and down-regulated gene programs: (C) MYB_Q6, (D) GSE9988_LPS_VS_VEHICLE_TREATED_MONOCYTES_UP, and (E) GERY_CEBP_TARGETS_377.
(F) Histogram of Annexin V- or CD11b-stained MV411 cell fluorescence, treated with CRYBMIM (red), MYBMIM (gray), or control PBS (black); * p < 1e-15, Kruskal-Wallis test.
(G) Scatter plots comparing Annexin V- versus CD11b-stained MV411 cell fluorescence, treated with control PBS, MYBMIM or CRYBMIM; blue to red color indicates increasing cell density.

Figure 4. CRYBMIM remodels MYB and CBP/P300 chromatin complexes in AML cells.
(A-B) Volcano plots of MYB chromatin occupancy changes after one hour (A) and four hours (B) of 20 μM CRYBMIM treatment compared to control, as analyzed by ChIP-seq. Sequence motifs found in CRYBMIM-induced MYB-depleted (left) and MYB-enriched loci (right) are shown. *p*-values denote statistical significance of 3 technical replicates.
(C-D) Volcano plots of CBP/P300 chromatin occupancy changes after one hour (A) and four hours (B) of 20 μM CRYBMIM treatment as compared to control, as analyzed by ChIP-seq. Sequence motifs found in CRYBMIM-induced of MYB-depleted (left) and MYB-enriched loci (right) are shown. *p*-values denote statistical significance of 3 technical replicates.

Figure 5. MYB assembles aberrant nuclear transcription factor complexes in AML cells.
(A) Volcano plot of nuclear MYB-associated proteins compared to IgG control, as analyzed by affinity purification-mass spectrometry of MV411 cells. Red symbols denote specifically MYB-associated proteins, with CBP/P300 as threshold (MYB/IgG $\log_2$>1). *p*-values denote statistical significance of 3 biological replicates.
(B) Enrichment of MYB-associated proteins (red) as a function of their corresponding CRISPR DepMap dependency scores in MV411 cells. Red symbols denote functionally required proteins, with CBP/P300 as threshold (score<-0.18).
(C) Network of BioGRID protein interactions for MYB-associated nuclear AML proteins as a function of their respective hematopoietic expression aberrancy scores, based on relative expression in normal bone human bone marrow progenitor cells (red).
(D) Comparison of dependency scores in leukemia cell lines as compared to all other non-hematopoietic cancer cell lines for MYB-associated nuclear AML proteins, with red symbols denoting proteins that are required in leukemia but as compared to non-hematopoietic cancers.

Figure 6. Chromatin dynamics of CRYBMIM remodeled transcription factor complexes in AML cells.
(A) Heatmap of transcription factor chromatin occupancy in MV411 cells as a function of time of control PBS or CRYBMIM treatment. Nine clusters identified using k-means clustering are marked by yellow (loss of MYB and CBP), purple (loss of CBP and gain of MYB), orange (gain of MYB and CBP), pink (gain of CBP), and blue (no apparent changes of MYB and CBP) boxes, based on the similarity of their *z*-scores, with red and blue representing enrichment or depletion of factors, respectively.
(B) Groups of clusters comprising similar responses to CRYBMIM treatment based on MYB and CBP/P300 dynamics. Sequence motifs enriched at specific loci for each cluster are listed. Factors in white denote factors presumed to be enriched based on sequence motif enrichment.

REFERENCES

Bell, C. C. *et al.* (2019) 'Targeting enhancer switching overcomes non-genetic drug resistance in acute myeloid leukaemia', *Nature Communications*, 10(1), p. 2723. doi: 10.1038/s41467-019-10652-9.

Bradner, J. E., Hnisz, D. and Young, R. A. (2017) 'Transcriptional Addiction in Cancer', *Cell*, 168(4), pp. 629–643. doi: 10.1016/j.cell.2016.12.013.

Brown, F. C. *et al.* (2017) 'Genomics of primary chemoresistance and remission induction failure in paediatric and adult acute myeloid leukaemia', *British Journal of Haematology*, 176(1), pp. 86–91. doi: 10.1111/bjh.14413.

Brown, F. C. *et al.* (2018) 'MEF2C Phosphorylation Is Required for Chemotherapy Resistance in Acute Myeloid Leukemia.', *Cancer discovery*, 8(4), pp. 478–497. doi: 10.1158/2159-8290.CD-17-1271.

Cancer Genome Atlas Research Network *et al.* (2013) 'Genomic and epigenomic landscapes of adult de novo acute myeloid leukemia.', *The New England journal of medicine*, 368(22), pp. 2059–74. doi: 10.1056/NEJMoa1301689.

Cheng, G. *et al.* (2017) 'Loss of p300 accelerates MDS-associated leukemogenesis', *Leukemia*, 31(6), pp. 1382–1390. doi: 10.1038/leu.2016.347.

Cheng, J. C. *et al.* (2008) 'CREB is a critical regulator of normal hematopoiesis and leukemogenesis.', *Blood*, 111(3), pp. 1182–92. doi: 10.1182/blood-2007-04-083600.

Dai, P. *et al.* (1996) 'CBP as a transcriptional coactivator of c-Myb', *Genes and Development*, 10(5), pp. 528–540. doi: 10.1101/gad.10.5.528.

Gonda, T. J. *et al.* (1993) 'Differentiation state and responses to hematopoietic growth factors of murine myeloid cells transformed by myb.', *Blood*, 82(9), pp. 2813–22.

Gonda, T. J., Buckmaster, C. and Ramsay, R. G. (1989) 'Activation of c-myb by carboxy-terminal truncation: relationship to transformation of murine haemopoietic cells in vitro.', *The EMBO journal*, 8(6), pp. 1777–83.

Goto, N. K. *et al.* (2002) 'Cooperativity in transcription factor binding to the coactivator CREB-binding protein (CBP): The mixed lineage leukemia protein (MLL) activation domain binds to an allosteric site on the KIX domain', *Journal of Biological Chemistry*, 277(45), pp. 43168–43174. doi: 10.1074/jbc.M207660200.

Greenblatt, S. M. *et al.* (2019) 'CARM1 Is Essential for Myeloid Leukemogenesis but Dispensable for Normal Hematopoiesis', *Cancer Cell*, 35(1), p. 156. doi: 10.1016/j.ccell.2018.12.008.

He, B. *et al.* (2019) 'Diverse noncoding mutations contribute to deregulation of cis-regulatory landscape in pediatric cancers', *bioRxiv*, p. 843102. doi: 10.1101/843102.

Hu, Y. L. *et al.* (1991) 'Transformation by carboxyl-deleted Myb reflects increased transactivating capacity and disruption of a negative regulatory domain', *Oncogene*, 6(9), pp. 1549–1553.

Jian, W. *et al.* (2017) 'Histone deacetylase 1 activates PU.1 gene transcription through regulating TAF9 deacetylation and transcription factor IID assembly', *The FASEB Journal*, 31(9), pp. 4104–4116. doi: 10.1096/fj.201700022R.

Jones, S. (2004) 'An overview of the basic helix-loop-helix proteins.', *Genome biology*, 5(6), p.

226. doi: 10.1186/gb-2004-5-6-226.

Kasper, L. H. *et al.* (2010) 'CBP/p300 double null cells reveal effect of coactivator level and diversity on CREB transactivation', *The EMBO Journal*, 29(21), pp. 3660–3672. doi: 10.1038/emboj.2010.235.

Kentsis, A. *et al.* (2012) 'Autocrine activation of the MET receptor tyrosine kinase in acute myeloid leukemia', *Nature Medicine*, 18(7), pp. 1118–1122. doi: 10.1038/nm.2819.

Klempnauer, K. H. and Bishop, J. M. (1984) 'Neoplastic transformation by E26 leukemia virus is mediated by a single protein containing domains of gag and myb genes.', *Journal of Virology*, 50(1), pp. 280–283. doi: 10.1128/jvi.50.1.280-283.1984.

Krivtsov, A. V. *et al.* (2019) 'A Menin-MLL Inhibitor Induces Specific Chromatin Changes and Eradicates Disease in Models of MLL-Rearranged Leukemia', *Cancer Cell*, 36(6), pp. 660-673.e11. doi: 10.1016/j.ccell.2019.11.001.

Lasko, L. M. *et al.* (2017) 'Discovery of a selective catalytic p300/CBP inhibitor that targets lineage-specific tumours', *Nature*, 550(7674), pp. 128–132. doi: 10.1038/nature24028.

Lei, W. *et al.* (2004) 'Positive and negative determinants of target gene specificity Myb transcription factors', *Journal of Biological Chemistry*, 279(28), pp. 29519–29527. doi: 10.1074/jbc.M403133200.

Look, A. T. (1997) 'Oncogenic Transcription Factors in the Human Acute Leukemias', *Science*, 278(5340), pp. 1059–1064. doi: 10.1126/science.278.5340.1059.

Luger, S. M. *et al.* (2002) 'Oligodeoxynucleotide-mediated inhibition of c-myb gene expression in autografted bone marrow: a pilot study.', *Blood*, 99(4), pp. 1150–8. doi: 10.1182/blood.v99.4.1150.

Mansour, M. R. *et al.* (2014) *An oncogenic super-enhancer formed through somatic mutation of a noncoding intergenic element*, *Science*. doi: 10.1126/science.1259037.

Meng, Y.-S. *et al.* (2005) 'Oncogenic potential of the transcription factor LYL1 in acute myeloblastic leukemia', *Leukemia*, 19(11), pp. 1941–1947. doi: 10.1038/sj.leu.2403836.

Ogiwara, H. *et al.* (2016) 'Targeting p300 Addiction in CBP-Deficient Cancers Causes Synthetic Lethality by Apoptotic Cell Death due to Abrogation of MYC Expression', *Cancer Discovery*, 6(4), pp. 430–445. doi: 10.1158/2159-8290.CD-15-0754.

Oughtred, R. *et al.* (2019) 'The BioGRID interaction database: 2019 update', *Nucleic Acids Research*, 47(D1), pp. D529–D541. doi: 10.1093/nar/gky1079.

Pattabiraman, D. R. *et al.* (2014) 'Interaction of c-Myb with p300 is required for the induction of acute myeloid leukemia (AML) by human AML oncogenes', *Blood*, 123(17), pp. 2682–2690. doi: 10.1182/blood-2012-02-413187.

Pattabiraman, D. R. and Gonda, T. J. (2013) 'Role and potential for therapeutic targeting of MYB in leukemia.', *Leukemia*, 27(2), pp. 269–77. doi: 10.1038/leu.2012.225.

Radhakrishnan, I. *et al.* (1997) 'Solution structure of the KIX domain of CBP bound to the transactivation domain of CREB: a model for activator:coactivator interactions', *Cell*, 91, pp. 741–752.

Ramaswamy, K. *et al.* (2018) 'Peptidomimetic blockade of MYB in acute myeloid leukemia', *Nature Communications*. Springer US, 9(1), p. 110. doi: 10.1038/s41467-017-02618-6.

Roe, J.-S. *et al.* (2015) 'BET Bromodomain Inhibition Suppresses the Function of Hematopoietic Transcription Factors in Acute Myeloid Leukemia', *Molecular Cell*, 58(6), pp. 1028–1039. doi: 10.1016/j.molcel.2015.04.011.

Sanda, T. *et al.* (2012) 'Core Transcriptional Regulatory Circuit Controlled by the TAL1 Complex in Human T Cell Acute Lymphoblastic Leukemia', *Cancer Cell*, 22(2), pp. 209–221. doi: 10.1016/j.ccr.2012.06.007.

Selvakumaran, M., Liebermann, D. A. and Hoffman-Liebermann, B. (1992) 'Deregulated c-myb disrupts interleukin-6- or leukemia inhibitory factor-induced myeloid differentiation prior to c-myc: role in leukemogenesis.', *Molecular and Cellular Biology*, 12(6), pp. 2493–2500. doi: 10.1128/MCB.12.6.2493.

Suzuki, K. *et al.* (2017) 'Recurrent MYB rearrangement in blastic plasmacytoid dendritic cell neoplasm', *Leukemia*, 31(7), pp. 1629–1633. doi: 10.1038/leu.2017.101.

Tarumoto, Y. *et al.* (2018) 'LKB1, Salt-Inducible Kinases, and MEF2C Are Linked Dependencies in Acute Myeloid Leukemia.', *Molecular cell*, 69(6), pp. 1017-1027.e6. doi: 10.1016/j.molcel.2018.02.011.

Tsherniak, A. *et al.* (2017) 'Defining a Cancer Dependency Map', *Cell*, 170(3), pp. 564-576.e16. doi: 10.1016/j.cell.2017.06.010.

Tyner, J. W. *et al.* (2018) 'Functional genomic landscape of acute myeloid leukaemia', *Nature*, 562(7728), pp. 526–531. doi: 10.1038/s41586-018-0623-z.

Uttarkar, S. *et al.* (2015) 'Naphthol AS-E phosphate inhibits the activity of the transcription factor Myb by blocking the interaction with the KIX domain of the coactivator p300', *Molecular Cancer Therapeutics*. doi: 10.1158/1535-7163.MCT-14-0662.

Uttarkar, S. *et al.* (2016) 'Targeting acute myeloid leukemia with a small molecule inhibitor of the Myb/p300 interaction', *Blood*. doi: 10.1182/blood-2015-09-668632.

Vakoc, C. R. and Kentsis, A. (2018) 'Disabling an oncogenic transcription factor by targeting of control kinases', *Oncotarget*, 9(64). doi: 10.18632/oncotarget.25971.

van der Meer, D. *et al.* (2019) 'Cell Model Passports—a hub for clinical, genetic and functional datasets of preclinical cancer models', *Nucleic Acids Research*, 47(D1), pp. D923–D929. doi: 10.1093/nar/gky872.

Wang, L. *et al.* (2011) 'The Leukemogenicity of AML1-ETO Is Dependent on Site-Specific Lysine Acetylation', *Science*, 333(6043), pp. 765–769. doi: 10.1126/science.1201662.

Xu, Y. *et al.* (2018) 'A TFIID-SAGA Perturbation that Targets MYB and Suppresses Acute Myeloid Leukemia', *Cancer Cell*, 33(1), pp. 13-28.e8. doi: 10.1016/j.ccell.2017.12.002.

Xu, Y. *et al.* (2019) 'TAF1 plays a critical role in AML1-ETO driven leukemogenesis', *Nature Communications*, 10(1), p. 4925. doi: 10.1038/s41467-019-12735-z.

Zhao, L. *et al.* (2011) 'Integrated genome-wide chromatin occupancy and expression analyses identify key myeloid pro-differentiation transcription factors repressed by Myb', *Nucleic Acids Research*, 39(11), pp. 4664–4679. doi: 10.1093/nar/gkr024.

Zor, T. *et al.* (2004) 'Solution Structure of the KIX Domain of CBP Bound to the Transactivation Domain of c-Myb', *Journal of Molecular Biology*, 337(3), pp. 521–534. doi: 10.1016/j.jmb.2004.01.038.

Supplemental Data

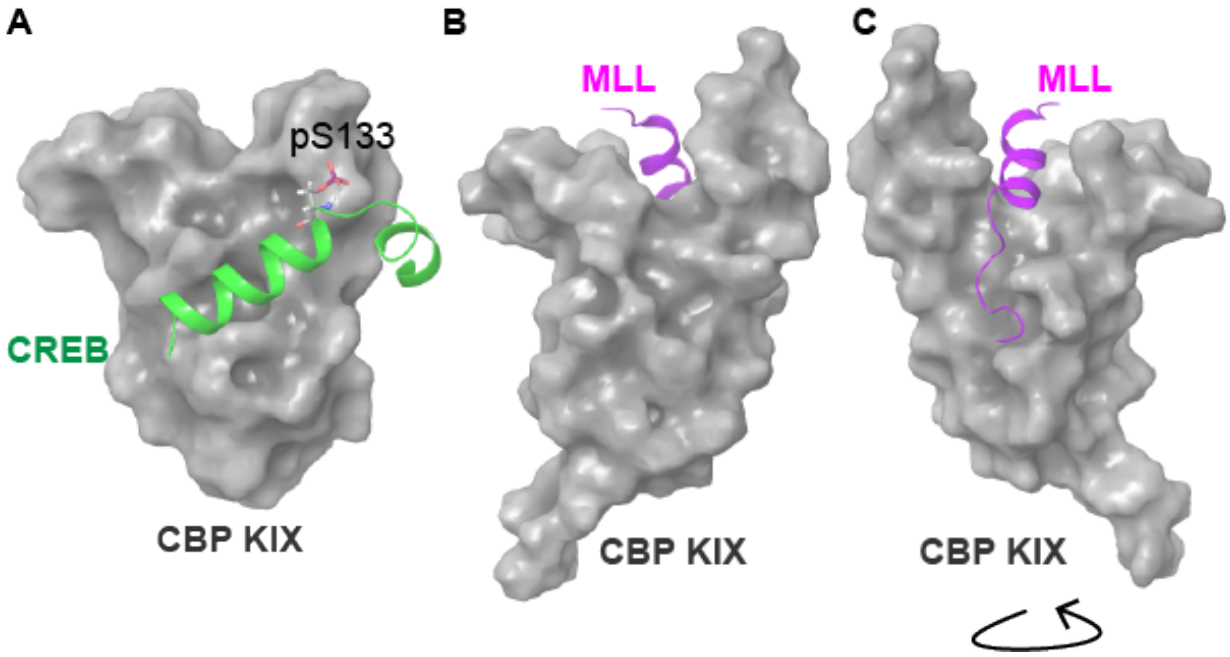

Figure S1. Molecular models of CREB and MLL structures in complex with CBP KIX. Related to Figure 1.

(A) Molecular model of the CREB:KIX complex assembled in Maestro (Schrödinger) using PDB 1KDX showing phosphor-Serine 133.

(B) Molecular model of the MLL:KIX complex assembled in Maestro (Schrödinger) using PDB 2LXS shown from the MYB/CREB binding site on KIX.

(C) Molecular model of the MLL:KIX complex assembled in Maestro (Schrödinger) using PDB 2LXS rotated to show the full MLL peptide.

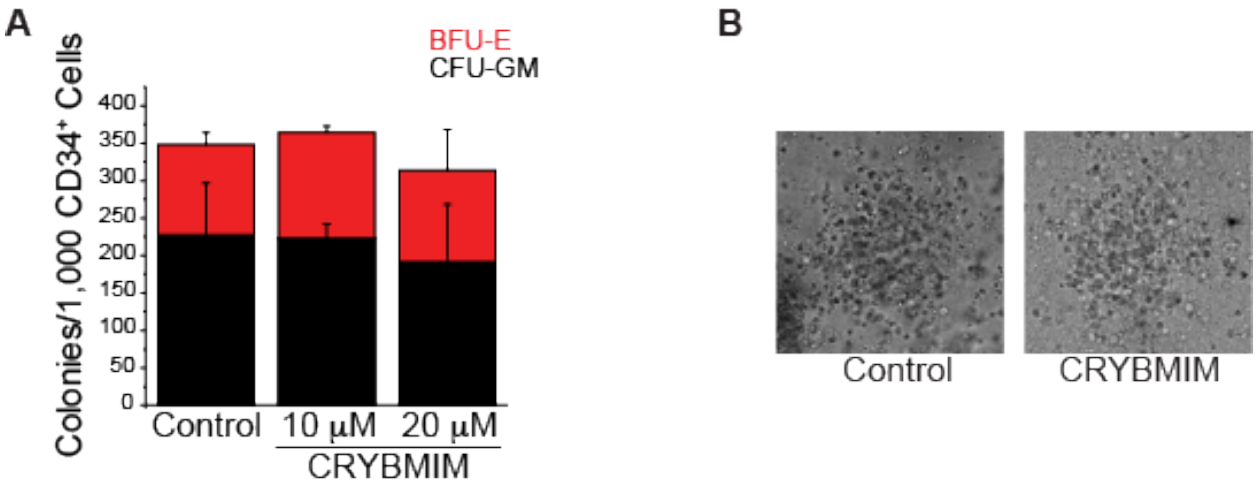

Figure S2. CRYBMIM spares normal hematopoietic progenitor cells in vitro. Related to Figure 3.

(A) Colony forming ability of CD34+ cells isolated from umbilical human cord blood following CRYBMIM treatment. BFU-E: Blast forming units – erythroid (red); CFU-GM: Colony forming units – granulocyte macrophage (black)

(B) Morphology of CD34+ cells isolated from umbilical human cord blood following 20 μM CRYBMIM treatment.

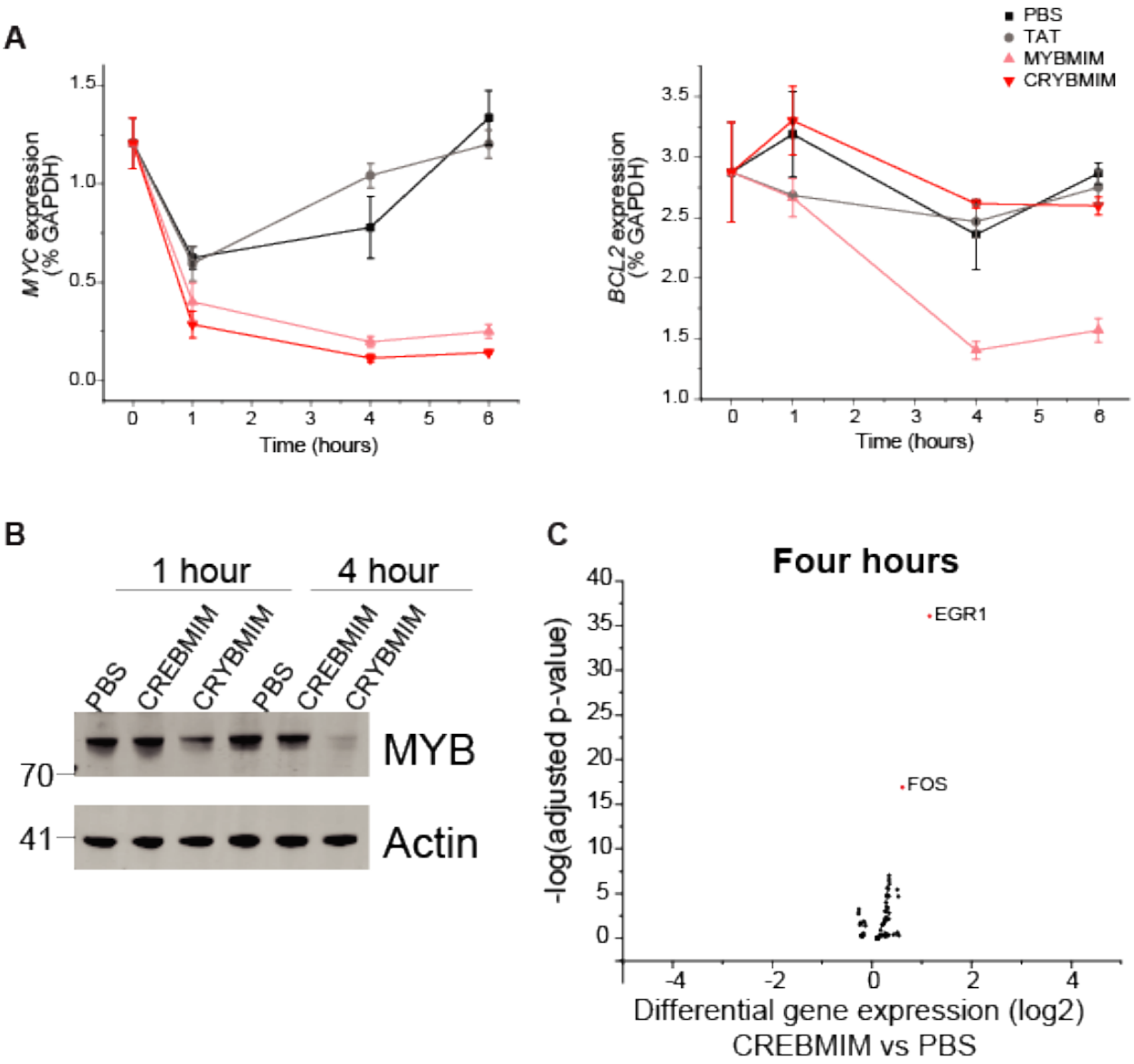

Figure S3. CRYBMIM but not CREBMIM causes significant changes in gene expression in AML cells upon short duration exposure. Related to Figure 3.

(A-B) Gene expression of MYB target genes *MYC* (A) and *BCL2* (B) in AML after 20 μM peptide treatment as measured by qPCR.

(B) Western blot of MYB following short duration 20 μM peptide treatment

(C) Gene expression changes in MV411 cells treated with 20 μM CREBMIM for 4 hours as measured by RNA-seq

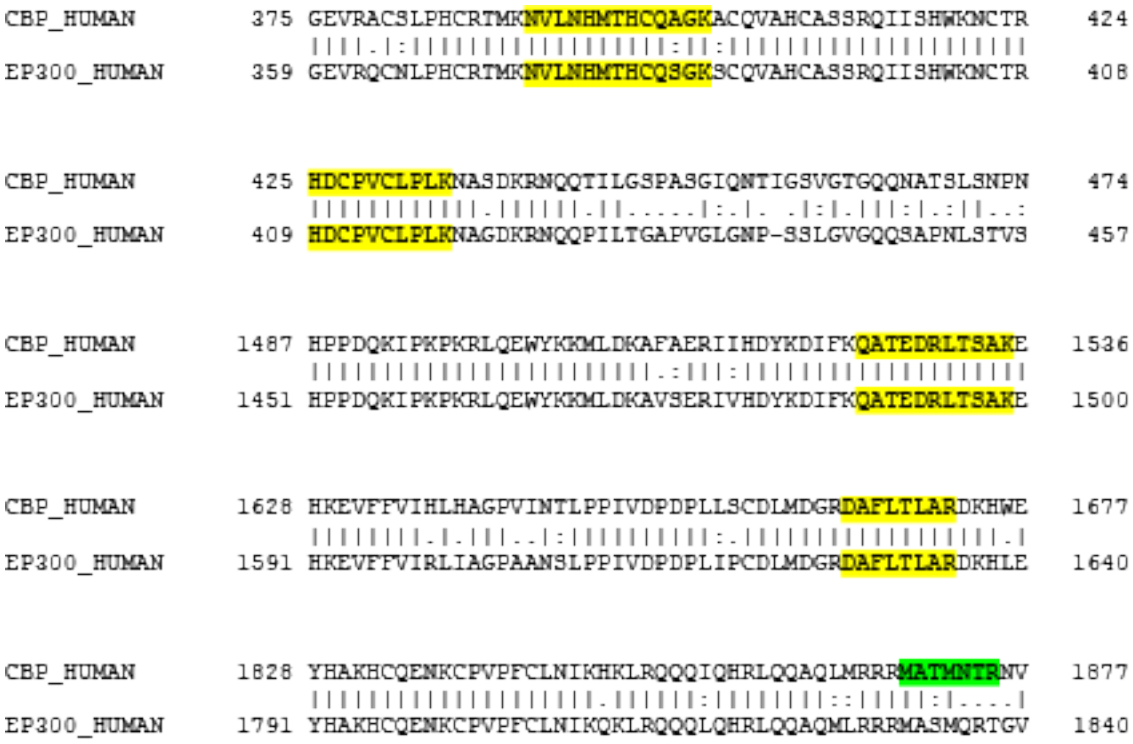

Figure S4. CBP rather than P300 is the primary binding partner of MYB in AML cells. Related to Figure 5.

Sequence alignment of relevant CBP (top row) and P300 (bottom row) amino acids. Highlighted peptides identified in mass spectrometry analysis aligned to either CBP only (green) or both CBP and P300 (yellow).

Supplementary Table 1

List of retro-inverso peptides with extinction coefficients. Related to Figure 1-2.

Peptide	Sequence	Extinction Coefficient ($M^{-1}cm^{-1}$)
MYBMIM	[Ac]-KLENETSMLLLELEKIRKGGRRRQRRKKRGY-[NH2]	1490
CREBMIM	[Ac]-GPADSSLDNLIKRYpSPRRSLIERRGGRRRQRRKKRGY-[NH2]	2980
CRYBMIM	[Ac]-KLENETSMLLLELKRYpSPRRSLIERRGGRRRQRRKKRGY-[NH2]	2980
CG3	[Ac]-KLGNETSMGLLELKRYGPRRSLIERRGGRRRQRRKKRGY-[NH2]	2980
TG3	[Ac]-KLGNETSMGLLELEKIGKGGRRRQRRKKRGY-[NH2]	1490
MLLMIM	[Ac]-TNKLVFDMIDSPLINGGRRRQRRKKRGY-[NH2]	1490
Bio-CREBMIM	[Ac]-GPADSSLDNLIKRYpSPRRSLIERRGGRRRQRRKKRGY-[K-Biotin]-[NH2]	2980
Bio-CRYBMIM	[Ac]-KLENETSMLLLELKRYpSPRRSLIERRGGRRRQRRKKRGY-[K-Biotin]-[NH2]	2980
FITC-CREBMIM	[Ac]-GPADSSLDNLIKRYpSPRRSLIERRGGRRRQRRKKRGY-[K-FITC]-[NH2]	75000 (FITC)
FITC-CRYBMIM	[Ac]-KLENETSMLLLELKRYpSPRRSLIERRGGRRRQRRKKRGY-[K-FITC]-[NH2]	75000 (FITC)
RI-TAT	[Ac]-RRRQRRKKRGY	1490

Supplementary Table 2

Mutational landscape of human AML cell lines determined by whole genome sequencing. Related to Figure 2.

AML cell line[a,b]	Known somatic short-variants (percent-reads, coverage)	Likely somatic short-variants (percent-reads, coverage)	High-level (CN>8) and focal (CN>5) amplifications of genes recurrently amplified in cancer (copy-number, exons)	Homozygous deletions of genes known to be recurrently deleted in cancer (0,exons)	Known functional rearrange-ments (gene1_gene2_genomic even description_supporting-reads)	Likely functional rearrange-ments (gene1_gene2_genomic event description_supporting-reads)
HL-60	NRAS_c.182A>T_p.Q61L(0.49,308),CDKN2A_c.238C>T_p.R80*(1.0,223)	TLL2_c.661C>T_p.R221*(0.52,434)	MYC_amplification(23,5 of 5)	TP53_loss(0,14 of 14)		
Kasumi-1	ASXL1_c.1934_1935insG_p.G646fs*12(0.35,555),TP53_c.743G>A_p.R248Q(1.0,320),KIT_c.2466T>A_p.N822K(0.82,1215),CDKN2A_c.172C>T_p.R58*(1.0,273)	SMARCA4_c.4109_4109delG_p.G1370fs*14(0.52,628),NCOR1_c.6011-1G>T_p.splice site 6011-1G>T(1.0,194),CREBBP_c.1676+1_1676+10del10_p.splice site 1676+1_1676+10del10(0.99,186)	KIT_amplification(12,21 of 21),KDR_amplification(12,30 of 30),PDGFRA_amplification(12,22 of 22)		RUNX1_RUNX1T1_fusion	
THP1	NRAS_c.35G>A_p.G12D(0.72,845)	TP53_c.518_543delTGAGGCGCTGCCCCCACCATGAGCGC_p.R174fs*3(0.96,337)	MYCL1_amplification(25,5 of 5)	CDKN2A_loss(0,5 of 5),PTEN_loss(0,6 of 9),CDKN2B_loss(0,5 of 5)	KMT2A_MLLT3_fusion_525	KMT2A_SNAPC3_rearrangement_230

OCI-AML2	DNMT3A_c.1903C>T_p.R635W(1.0,521),TP53_c.659A>G_p.Y220C(0.01,592),FLT3_c.2039C>T_p.A680V(0.49,449)	SPEN_c.4798A>T_p.K1600*(0.5,581),SPEN_c.8675_8676delCA_p.T2892fs*2(0.49,804),ZRSR2_c.1343_1344insGAGCCG_p.R448_R449insSR(0.49,267)				
MV411	POT1_c.115A>G_p.K39E(0.37,394)	FLT3_c.1771_1772insACGTTGATTTCAGAGAATATGAATATGATC_p.Y591_V592insVDFREYEYDH(0.56,947)			KMT2A_AFF1_fusion_2799	
MOLM13		FLT3_c.1774_1775insTTGATTTCAGAGAATATGAAT_p.V592_D593insDFREYEF(0.49,942)		CDKN2A_loss(0,5 of 5),CDKN2B_loss(0,5 of 5)	MLL_MLLT3_fusion_78	
HEL	JAK2_c.1849G>T_p.V617F(1.0,1448),TP53_c.398T>A_p.M133K(1.0,400)	PASK_c.3909_3910insG_p.E1305fs*4(0.61,456)	CD274_amplification(9,7 of 7),PDCD1LG2_amplification(15,6 of 6),JAK2_amplification(15,23 of 23)	CDKN2A_loss(0,5 of 5),CDKN2B_loss(0,5 of 5)		KEAP1_NOTCH3_rearrangement_603
K562	TP53_c.404_405insC_p.Q136fs*13(0.91,386)	ASXL1_c.1773C>A_p.Y591*(0.33,593)	MAPK1_amplification(19,8 of 8),CRKL_amplification(16,5 of 5)	CDKN2A_loss(0,5 of 5),CDKN2B_loss(0,5 of 5)	BCR_ABL1_fusion_1295	

U937	WT1_c.1105C>T_p.R369*(0.53,204),PTPN11_c.178G>C_p.G60R(0.53,319),JAK3_c.1533G>A_p.M511I(0.66,486)	MAP3K6_c.1731_1736+5del11_p.splice site 1731_1736+5del11(0.27,753),PTEN_c.389_390insCCCG_p.T131fs*50(0.86,165),TP53_c.559+1G>A_p.splice site 559+1G>A(1.0,432)		HDAC4_loss(0,2 of 26)		ETV6_ETV6_deletion_62
NB-4	FGFR3_c.746C>T_p.S249F(0.39,1063),TP53_c.743G>A_p.R248Q(1.0,427)	KRAS_c.53C>A_p.A18D(0.74,918)	CD274_amplification(7,7 of 7),KDM4C_amplification(7,25 of 25),KRAS_amplification(7,5 of 5),MYC_amplification(13,5 of 5),PDCD1LG2_amplification(7,6 of 6)	CDKN2A_loss(0,5 of 5),CDKN2B_loss(0,5 of 5)	RARA_PML_fusion_287	
OCI-AML3	NRAS_c.182A>T_p.Q61L(1.0,361),NPM1_c.863_864insTCTG_p.W288fs*10+(0.38,245),DNMT3A_c.2644C>T_p.R882C(0.46,482)					ETV6_ETV6_truncation_159
SKM1	KRAS_c.351A>C_p.K117N,TP53_c.743G>A_p.R248Q,TET2_c.4253_4254insTT_p.P1419fs*30,STAG2_c775C>T_p.					

	R259*,SPTAN1_c.351A>C_p.Q959*,EZH2_c.1937A>G_p.Y646C,BCOR_c4977-1G>A_p?,ASXL1_c.1773C>A_pY591*					

a (Brown *et al.*, 2017)

b (van der Meer *et al.*, 2019)

Supplementary Table 3

Summary of Gene Set Enrichment Analysis on CRYBMIM-induced differentially expressed genes, as measured by RNA-sequencing. Related to Figure 3.

1 HOUR CRYBMIM

Up-regulated	**NES**	**FDR q-val**
HALLMARK_TNFA_SIGNALING_VIA_NFKB	2.8024669	0
GSE9988_ANTI_TREM1_VS_CTRL_TREATED_MONOCYTES_UP	2.5309677	0
GSE9988_LPS_VS_VEHICLE_TREATED_MONOCYTE_UP	2.472586	0
PID_AP1_PATHWAY	2.420644	0
HESS_TARGETS_OF_HOXA9_AND_MEIS1_DN	2.3865807	0
MORF_JUND	2.3207855	1.78E-05
PID_ATF2_PATHWAY	2.308911	3.43E-05
GO_CHROMATIN_SILENCING	2.2787592	7.48E-05
GNF2_FOS	2.2453063	1.70E-04
GO_NEGATIVE_REGULATION_OF_GENE_EXPRESSION_EPIGENETIC	2.171959	6.48E-04
REACTOME_ACTIVATION_OF_THE_AP1_FAMILY_OF_TRANSCRIPTION_FACTORS	2.0386379	0.004558261
WANG_LSD1_TARGETS_DN	2.0096538	0.006502762
ONO_AML1_TARGETS_UP	1.9874691	0.008697852
TAVOR_CEBPA_TARGETS_UP	1.9762611	0.009819131
GERY_CEBP_TARGETS	1.974775	0.010005118
BIOCARTA_ETS_PATHWAY	1.9510418	0.012995631
PID_P53_DOWNSTREAM_PATHWAY	1.9154657	0.018464027
HALMOS_CEBPA_TARGETS_UP	1.8936123	0.02239665
Down-regulated	**NES**	**FDR q-val**
MYB_Q6	-1.6279523	0.4027038

4 HOUR CRYBMIM

Up-regulated	**NES**	**FDR q-val**
HALLMARK_TNFA_SIGNALING_VIA_NFKB	2.6672592	0
GSE9988_ANTI_TREM1_AND_LPS_VS_CTRL_TREATED_MONOCYTES_UP	2.5861802	0
GSE9988_LPS_VS_VEHICLE_TREATED_MONOCYTE_UP	2.561319	0
HALMOS_CEBPA_TARGETS_UP	2.297455	0
GO_MONOCYTE_CHEMOTAXIS	2.2337112	0
GO_GRANULOCYTE_MIGRATION	2.2233214	0
GO_LEUKOCYTE_CHEMOTAXIS	2.2228014	0
PID_AP1_PATHWAY	2.2088113	0
DASU_IL6_SIGNALING_UP	2.2057369	0
HESS_TARGETS_OF_HOXA9_AND_MEIS1_DN	2.196779	0
GO_MYELOID_LEUKOCYTE_MIGRATION	2.1960723	0
GO_CHROMATIN_SILENCING	2.176191	0
GERY_CEBP_TARGETS	2.151518	0
ONO_AML1_TARGETS_UP	2.0420718	3.16E-05
HALLMARK_APOPTOSIS	2.0164626	9.41E-05
HALLMARK_P53_PATHWAY	1.9541126	4.20E-04
MORF_JUND	1.9532294	4.24E-04
BIOCARTA_ETS_PATHWAY	1.9100726	0.001063434
GNF2_FOS	1.9015049	0.001225544
Down-regulated	**NES**	**FDR q-val**
HALLMARK_E2F_TARGETS	-2.731907	0
HALLMARK_MYC_TARGETS_V2	-2.367546	6.24E-05
SCHUHMACHER_MYC_TARGETS_UP	-2.2255418	3.28E-04
KAMMINGA_EZH2_TARGETS	-2.019596	0.004882885
IVANOVA_HEMATOPOIESIS_INTERMEDIATE_PROGENITOR	-1.9172059	0.013133204

Table S4. List of proteins identified by IP-MS of IgG control and MYB complex purifications from MV411 cell nuclei. Related to figure 5.

Table S5. MYB complex functional groups. Related to Figure 5.

Table S6. Pathway analysis of transcription factor-remodeled loci in response to CRYBMIM. Related to Figure 6.